Study of selenium solubility and speciation in groundwater

Reisuke DOI

January, 2014

Doctor thesis

Study of selenium solubility and speciation in groundwater

Deep Geological Environment Science (Jointly Offered Course)
Division of Material Sciences
Graduate School of Natural Science and Technology
Kanazawa University

Student ID number: 1323132005
Name: Reisuke Doi
Major doctoral adviser: Gento Kamei

Contents

Chapter 1. General introduction

1.1 Radioactive waste management

The world-wide use of nuclear energy generates considerable amount of radioactive waste [1, 2, 3]. The radioactive waste must be isolated until its radioactivity decays to an insignificant level. The geological disposal is world-wide recognized as the most successful procedure of the radioactive waste disposal. The feasibility of geological disposal is being studied world-wide. On the concept of the geological disposal, for the purpose of isolating them from environment, the high-level radioactive waste (HLW) will be vitrified and stored to cool for several decades, then located in deep geologic formations, where the vitrified waste is covered with over-pack and buffer material to provide an adequate long-term containment of radionuclides. This engineered barrier system will be combined with the massive structures of rock formation as a natural barrier to retard the radionuclide transport before reaching biosphere. A multi-barrier system consisting of the engineered barrier and the natural barrier is especially important for a long-lived radionuclide with a half-life of a few hundred thousand years.

Post-closure radiological safety assessments hinge on the ability to predict accurately the possible rate and extent of geochemical transport from a radioactive waste repository to man’s immediate environment. Groundwater is the transport media for radionuclides relevant to the safety assessment of the geological disposal system. Saturated bentonite buffer material has a homogeneous structure with microscopic pores. Because of its low permeability, nuclides leached from the vitrified waste will be transported by diffusion. In general, diffusion in solution is defined as a process by which solutes are transported from a high concentration region to a low concentration region as a result of random molecular motion.

The solubilities of elements limit the concentation gradients driving diffusion through the buffer. Most of the safety-relevant radioelements have low solubility under the expected reducing conditions. The concentration of radioelements will tend to increase with time due to leaching from the vitrified waste and ingrowth from parent nuclides. As a result, a solid phase containing radionuclides can be formed due to precipitation when the concentration of radioelement will exceed its solubility and chemical equilibrium will exist between the precipitated solid phase and the groundwater. At that time, the solubility of the solid phase will govern the concentration of radionuclides in the groundwater. Laboratory tests [4, 5] have confirmed that the concentrations of poorly soluble elements leached from vitrified waste are limited by solubility of the precipitated solid phase.

The radionuclide transport will be retarded by sorption on to mineral surfaces. Each aqueous species will vary in its tendency to diffuse and sorb depending on size, charge and steric considerations. Speciation may be defined as the different chemical forms of an element which together comprise its total concentration in a given environment [6]. Speciation data are required to predict the mobility of radionuclides from radioactive waste repositories.

Thus, a knowledge of solubility and speciation is essential to understanding the possible migration behaviour of a radionuclide in any disposal situation and estimating the dose corresponding to nuclides releases to the biosphere. Thermodynamic models assuming that equilibrium conditions persist are used to calculate solubility and speciation as functions of pH, redox potential, *E*, and ligand concentrations. In the calculation of solubility and speciation, the reliability of the results is necessarily dependent on that of available thermodynamic data and the validity of the choice of the solubility-limiting solid phase. The importance of the development of reliable thermodynamic databases for the safety assessments of the geological disposal system

has been internationally recognized; The Organization for Economic Cooperation and Development sponsored the Nuclear Energy Agency chemical thermodynamics project (OECD/NEA). The choice of the solubility-limiting solid phase must be made carefully, respecting thermodynamic stability and experimental findings.

1.2 Solubility and speciation of Se

Selenium-79(^{79}Se) is a long-lived fission product with a half-life of 327,000 years [7]. Se is ubiquitous in geologic environments and is an essential micronutrient, yet it promotes toxicity and adverse biologic effects at relatively low concentrations [8]. Se aqueous species in groundwater are present as anions. Sorption of Se aqueous species on to buffer material and a host rock is relatively small, which results in only slight retardation of Se relative to groundwater movement. Therefore, Se is one of the key radionuclides for the safety assessment of the geological disposal system. The oxidation state of Se varies from Se(−II) to Se(VI), depending on the redox conditions of groundwater. The stability ranges of the predominant Se species in aqueous systems are summarized and displayed in Figure 1 [9]. The thermodynamic calculations indicate that the predominant Se oxidation state is Se(0), Se(−II) and Se_n^{2-} (n = 1, 2, 3 and 4) at low *E* values, Se(VI) at high *E* values and Se(IV) in the intermediate environmental range of *E* values. Each oxidation state of Se has unique solubility, sorption and complexation chemistry, which dictate its migration behavior in the environment. In general, Se(VI) has a high solubility and is the most mobile in water. Se(IV) is soluble in water but its strong affinity to be adsorbed to soil particles greatly reduces its mobility. Elemental selenium exists in a crystalline form. The migration behavior of Se can be significantly altered due to the oxidation/reduction potentials of the geologic environments. *E* is the most important parameter determining the migration behavior of Se.

1.3 Contents of this thesis

Groundwater flowing through deep geologic formations is likely to be weakly alkaline (pH = 8 ± 1) and reducing (E = −250 ± 50 mV vs. SHE) [10]. It is necessary to gauge the sensitivity of the system to perturbations in environmental conditions. Uplift, subsidence and erosion were considered to be potential natural phenomena related to the long-term stability of geological environments [10]. Radiolysis of groundwater due to radiation from the vitrified waste will generate oxidizing agents, such as H_2O_2 [10]. A decrease in the depth of repositories and the presence of oxidizing agents are of particular concern for the anticipated reducing conditions of repositories.

As mentioned in section 1.1, the reliability of the thermodynamic data and the choice of appropriate solubility-limiting solid phase are of key importance in the calculation of solubility and speciation using thermodynamic models. Therefore, the purpose of this thesis is to obtain 1) the critically important thermodynamic data for Se, and 2) the information on the solubility-limiting solid phase of Se. As mentioned in section 1.2, the migration behavior of Se significantly depends on E, emphasizing the need to estimate the solubility and speciation of Se in oxidized groundwater due to perturbations in the environment as well as in reducing groundwater.

In Chapter 2, in order to obtain the information on the solubility-limiting solid phase of Se under reducing conditions, the process of the identification of this solid phase was stated on the basis of the batch Se solubility experiments and thermodynamic calculations.

In Chapter 3, in order to obtain the thermodynamic data for the Se(VI)/(IV) couple, which determine the speciation of Se in oxidized groundwater, the process of determining these data was stated on the basis of the electrochemical investigations, using cyclic voltammetry. Conventionally, thermodynamic data are quoted for

"standard" conditions, i.e., 298 K, 1 bar pressure and zero ionic strength (infinite dilution). The activities of all the species participating in reactions must be estimated in order to convert the thermodynamic data obtained at different ionic strengths to zero ionic strength. One method for estimating the activities is through the use of the ion interaction parameters ($\varepsilon_T(i, j)$) in the specific ion interaction theory (SIT) model [11] to calculate the ion activity coefficients (γ_i). SIT was used in OECD/NEA [11] and Japan Atomic Energy Agency Thermodynamic Data Base review [12]. In Chapter 3, using SIT, the thermodynamic values were evaluated as a function of ionic strength.

References in Chapter 1.

1. Silva RJ, Nitsche H. [Actinide environmental chemistry]. Radiochim. Acta 1995; 70/71: 377.
2. Lieser KH. [Radionuclides in geosphere: sorces, mobility, reactions in natural waters and interactions with solids]. Radiochim. Acta 1995; 70/71: 355.
3. Fuger J. [Thermodynamic properties of actinide aqueous species relevant to geochemical problems]. Radiochim. Acta 1992; 58/59: 81.
4. Rai D, Felmy AR, Fulton RW, Ryan JL. [Aqueous chemistry of Nd in borosilicate-glass/water systems]. Radiochim. Acta 1992; 58/59:9-16.
5. Ashida T, Kohara Y, Yui M. [Migration behavior of Pu released from Pu-doped glass in compacted bentonite]. Radiochim. Acta 1994; 66/67:359-362.
6. Cross JE et al. Plutonium Speciation from Disposal Vault to Man. Weinheim: In A V Xavier and M G Weller (editors), Bioinorganic Chemistry VCH Publishers; 1985.
7. Jorg G, Buhnemann R, Hollas S, Kivel N, Kossert K, Van Winckel S, Gostomski CL. [Preparation of radiochemically pure ^{79}Se and highly precise determination of its half-life]. Appl. Radiat. Isotopes. 2010; 68:2339-2351.
8. Frankenberger Jr WT, Ensberg RA. Environmental Chemistry of Selenium. New York: Maecel Dekker Inc; 1998.
9. Olin Å, Noläng B, Öhman LO, Osadchii EG, Rosén E. Chemical Thermodynamics of Selenium. Amsterdam: ELSEVIER; 2005.
10. Japan Nuclear Cycle Development Institute (JNC). H12: Project to establish the scientific and technical basis for HLW disposal in Japan - second progress report on research and development for the geological disposal of HLW in Japan. Japan: Japan Nuclear Cycle Development Institute (JNC); 2000.

11. Grenthe I, Mompean F, Spahiu K, Wanner H. TDB-2 guidelines for the extrapolation to zero ionic strength. Issy-les-Moulineaux (France): OECD Nuclear Energy Agency; 2013. Available from: http://www.oecd-nea.org/dbtdb/guidelines/tdb2.pdf
12. Kitamura A, Fujiwara K, Doi R, Yoshida Y, Mihara M, Terashima M, Yui M. JAEA thermodynamic database for performance assessment of geological disposal of high-level radioactive and TRU wastes. Japan: Japan Atomic Energy Agency (JAEA); 2009.

Figure in Chapter 1

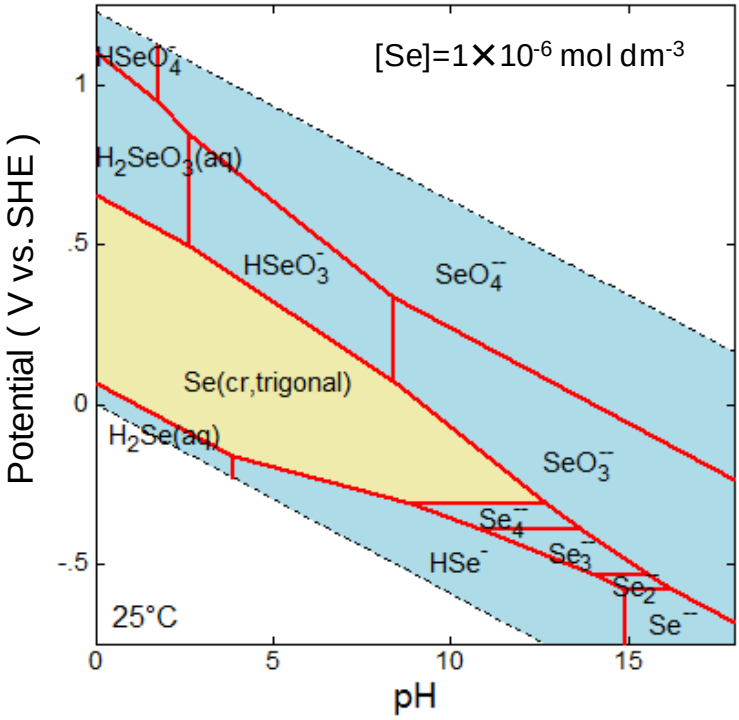

Figure 1. Potential-pH diagram for Se system based on the thermodynamic data reviewed and compiled by Olin et al. [9]. The total concentration of Se is 1×10^{-6} mol dm^{-3}.

Nomenclature

a_i : activity of ion *i*

γ_i : activity coefficient of ion *i*

z_i : charge of ion *i*

m_i : molality of ion *i* (amount of ion *i* divided by the mass of the solvent, mol kg^{-1})

[*i*] : molarity or concentration of ion *i* (amount of ion *i* divided by the volume of the solution, mol dm^{-3})

T : absolute temperature (T_0 = 298.15 K)

I_m : ionic strength of the working solution ($I_m = \frac{1}{2}\sum_i m_i z_i^2$, mol kg^{-1})

I_{Ref} : ionic strength of a solution contained in the reference electrode (mol kg^{-1})

$D(T, I_m)$: Debye-Hückel term (values of the Debye-Hückel constants taken from Olin et al. [9])

$\varepsilon_T(i, j)$: ion interaction coefficient between ion *i* and ion *j* of opposite charge (kg mol^{-1})

E : oxidation/reduction potential

$E_{\mathrm{Ox/Red}}(T, 0)$: standard redox potential of the Ox/Red couple

$E_{\mathrm{Ref}}(T, I_{\mathrm{Ref}})$: potential of the reference electrode

$E_p(\mathrm{Ox})$: anodic peak potential against the reference electrode

$E_p(\mathrm{Red})$: cathodic peak potential against the reference electrode

$E_{1/2}(T, I_m)$: half-wave potential [$E_{1/2}(T, I_m) = \{E_p(\mathrm{Ox}) + E_p(\mathrm{Red})\}/2$]

J : $RT/2F\log e$ (= 0.02958 V at 25.0 °C)

E (V vs. SCE) : potential against the saturated calomel reference electrode with a saturated solution of potassium chloride (KCl)

E(V vs. Hg/HgO): potential against the mercury-mercuric oxide reference electrode with a 0.1 mol dm^{-3} solution of sodium hydroxide (NaOH)

E (V vs. Ag/AgCl) : potential against the silver-silver chloride reference electrode with a saturated solution of KCl

E (V vs. SHE) : potential against the standard hydrogen electrode

K : the equilibrium constant of reaction

$\Delta_r G^0_m$: the molar Gibbs energy of reaction (kJ mol^{-1})

$\Delta_r H^0_m$: the molar enthalpy of reaction (k mol^{-1})

$\Delta_r S^0_m$: the molar entropy of reaction (J K^{-1} mol^{-1})

$\Delta_r C^0_{p,m}$: the molar heat capacity of reaction (J K^{-1} mol^{-1})

$\Delta_f G^0_m$: the standard molar Gibbs energy of formation from the elements in their reference states (kJ mol^{-1})

$\Delta_f H^0_m$: the standard molar enthalpy of formation from the elements in their reference states (kJ mol^{-1})

v : scan rate (V s^{-1})

σ : standard deviation

Chapter 2. Estimation of Se solubility in reducing groundwater

2.1 Introduction

As mentioned in section 1.3, repository environments are likely to be under reducing conditions. Fe(II), derived from carbon steel overpack corrosion, probably dissolves into bentonite porewater. Thermodynamic calculations indicate the likely formation of Fe-Se solid phases. In the recent R&D progress report for HLW disposal in Japan [1], $FeSe_2$(cr) was selected as the most thermodynamically stable solid phase in bentonite porewater. The prediction that $FeSe_2$(cr) limits the solubility of Se was thought to be valid in this report because sulfur (S) is a homologous element of Se and pyrite (FeS_2), which exists in bentonite, was assumed to be in equilibrium with the bentonite porewater. However, the low Se concentration limited by Fe-Se solids has not been observed in laboratory solubility experiments. Shibutani et al. [2] conducted Se solubility experiments at room temperature with solutions oversaturated with respect to $FeSe_2$(cr) for 4 weeks. However Fe-Se solids did not precipitate, instead Se(cr) was formed and limited the Se concentrations. $FeSe_2$(cr) may not form at room temperature because FeS_2 is formed at higher temperatures [3]. In the Se solubility experiments with solutions undersaturated and oversaturated with respect to $FeSe_2$(cr) for 8 months conducted by Iida et al. [4], the Se concentration was not limited by $FeSe_2$(cr), in spite of the precipitation of $FeSe_2$(cr). Andreas and Laurent [5] studied Se adsorption and reduction in the presence of FeS, $FeCO_3$ and Fe_3O_4 in a one-day experiment and they did not observe the thermodynamically most stable $FeSe_2$. Lee et al. [6] suggested that 2 weeks was insufficient to completely convert soluble Se to a solid phase under reducing condition and in the presence of Fe(II). So Se solubility and the solubility-limiting solid phase remains unclear despite numerous laboratory based investigations.

In order to determine the Se solubility-limiting solid, more information about Se solid phases is necessary. The purpose of Doi et al. [7] was to obtain such information by conducting a number of batch experiments supported by thermodynamic calculations. Batch Se solubility experiments were run at 60 and 80 °C under reducing conditions by the addition of excess Fe(II) and periodically sampled up to 3.5 months, with the main focus being on the Se concentrations in solution and Se solid phase characterization. Experiments in bentonite equilibrated waters as a more representative geological repository environment and a simple condition experiment without bentonite were performed.

2.2 Experimental

Two experiments were carried out in duplicate under an argon atmosphere inside a glove box (O_2 < 1 ppm). The first used bentonite equilibrated water and the second pure water. A summary of the experimental conditions is shown in Table 2. 1.

2.2.1 Experiments in bentonite equilibrated waters

Bentonite (Kunigel V1®, Kunimine Industries Co. Ltd) and Fe powder (Soekawa Chemical Company, 80–100 μm grain diameter) for maintaining reducing conditions were added to degassed ultrapure water and aged for 2 weeks. The supernatant was passed through a membrane-filter (pore size: 0.45 μm) and part of the filtrate was additionally passed through an ultra-filter (MWCO: 10,000). For both filtrates, metal ions and silicon concentrations were determined by an inductively coupled plasma atomic emission spectrometry (ICP-AES, Perkin Elmer Optima 3000) and anion concentrations by an ion chromatography and a total organic carbon analysis (Table 2. 2). The solution compositions of anion species after membrane-filtration should be the same as that after ultra-filter filtration, assuming the sorption of anion species on

bentonite colloids was negligible. For this reason, the solution compositions of anion species after membrane-filtration were not measured. The bentonite equilibrated water and Fe powder, as the reducing agent, were poured into a glass vessel. SeO_2 (Kanto Chemical Company) was dissolved in degassed ultrapure water and was used as the Se stock solution containing SeO_3^{2-}. The Fe(II) stock solution was prepared by the dissolution of Fe plate (Soekawa Chemical Company) in hydrochloric acid (HCl). Appropriate volumes of the Se stock solution and the Fe(II) stock solution were added to the bentonite-equilibrated water. Reducing conditions were maintained by adding Fe powder and Fe plate (Soekawa Chemical Company, 20 × 10 × 1 mm). The values of pH were adjusted to around 7 and 9 by the addition of sodium hydroxide (NaOH), or dilute HCl and the potential measured. Samples were then aged for 1 to 3 months at 60 °C. After the pH and potential were measured, the experimental solution was separated by centrifugation (15,000 rpm, 30 min). The supernatant was passed through a membrane-filter and the precipitate was analyzed by a X-ray diffractometer (XRD, Rigaku RINT). The filtrate was additionally passed through an ultra-filter and Se concentration determined by an inductively coupled plasma mass spectrometry (ICP-MS, Perkin Elmer ERAN 5000A). All samples were filtered at room temperature.

2.2.2 Experiments in pure waters (solid phase transformation experiment)

The Se stock solution was prepared by the dissolution of Se(cr) in 14 N NaOH (Kanto Chemical Company) solution at 80 °C and passing through a membrane-filter (pore size: 0.45 μm). The Fe(II) stock solution was prepared by the dissolution of Fe powder in HCl. Se and Fe concentrations were determined by the ICP-AES. Aliquots of both stock solutions were added to degassed ultrapure water in which the Fe powder, again acting as a reducing agent, was present. In order to identify the Se solid phase by the XRD, the excess Fe powder had to be kept separate from the precipitate by packing

the Fe powder into a cellulose tube (VISKASE sales corp.) tied on both sides by plastic wire, shown in Figure 2. 1. Both initial Se and Fe concentrations were 0.01 mol dm^{-3}. The Fe plate was added as a reducing agent. The values of pH were adjusted to 5 and 7 by the addition of NaOH or dilute HCl. The samples were aged for 1 to 3.5 months at 80 °C. After passing through an ultra-filter, Se concentrations in the filtrate were determined by the ICP-MS with an ultra-sonic nebulizer (USN), while the Fe concentrations were determined by the ICP-AES. The precipitate was separated by a membrane-filter and was characterized by the XRD. All samples were filtered at room temperature.

2.3 Results and discussion

2.3.1 Experiments in bentonite equilibrated waters

The XRD pattern of the solid phase after aging 3 months at pH value of 7 is shown in Figure 2. 2. Quartz derived from bentonite and Fe compounds accounted for most of the solid phase but no Se solid phases were identified.

Se concentrations, pH and potential are shown in Table 2. 3, which are plotted on potential-pH diagrams in Figure 2. 3, to identify the possible dominant aqueous species (Figure 2. 3. (a)) and the stable solid phases (Figure 2. 3. (b)). These diagrams are based on the thermodynamic data for Se reviewed and compiled by OECD/NEA [8]. The potential-pH diagram to identify the possible dominant aqueous species (Figure 2. 3. (a)) is restricted to 25 °C since there are no data for $\Delta_f H^0_m$ of the aqueous specie Se_4^{2-}. The thermodynamic data of Se(cr), Se(monocrystal), whose crystal axis has the same direction everywhere, and Se gas species were suppressed because these Se species dominate the potential-pH diagram, thereby allowing the prediction of aqueous Se species. According to the potential-pH diagram (Figure 2. 3. (a)), HSe^- would exist as

the dominant aqueous species under these experimental conditions, although Se_4^{2-} would also exist for samples 1-3 and 1-4.

The potential-pH diagram to identify the possible stable solid phases (Figure 2. 3. (b)) is restricted to 60 °C. To make the potential-pH diagram reliable at 60 °C, $\Delta_r H^0_m$ for some reactions are also taken into account. Values of log *K* at 60 °C (Table 2. 4) are adopted as additional input in the thermodynamic data for Se reviewed and compiled by OECD/NEA. There are no data for FeSe(cr) and for $FeSe_2$(cr) in this database because thermodynamic data for these species had not been critically reviewed following NEA-TDB Guidelines. However OECD/NEA selected the best values available for $\Delta_f G^0_m$ of $FeSe_2$(cr). The values of $\Delta_f H^0_m$ and log *K* for $FeSe_2$(cr) derived from $\Delta_f G^0_m$ of $FeSe_2$(cr) selected by OECD/NEA are used. The initial Fe concentrations are used to make the potential-pH diagram (Figure 2. 3. (b)) since Fe concentrations were not measured in the final solution. According to the potential-pH diagram (Figure 2. 3. (b)), the experimental conditions fell into the $FeSe_2$(cr) stability field, although the experimental conditions for sample 2-3 and 2-4 are plotted near the boundary between FeSe(cr) and $FeSe_2$(cr) stability fields. $FeSe_2$(cr) was recognized as the stable solid phase.

2.3.2 Experiments in pure waters (solid phase transformation experiment)

XRD patterns are shown in Figure 2. 4. After 1 month, the dominant solid phase was Se(cr). After aging for 3.5 months, the samples with initial pH values of about 5, showed a decrease in the amount of Se(cr) and an increase in the Fe-Se solid phases ($FeSe_2$(cr) and FeSe(cr)). In the experiments with initial pH values of about 7, Se(cr) gradually decreased with formation of Fe-Se solid phases. After 2 and 3.5 months aging, Se(cr) transformed to Fe-Se solid phase ($FeSe_2$(cr) and FeSe(cr)).

Values of potential, pH and concentrations of Fe and Se of the solutions are

shown in Table 2. 5. The experimental conditions shown in Table 2. 5 are plotted on potential-pH diagrams (Figure 2. 5) to identify the possible dominant aqueous species (Figure 2. 5. (a)) and the stable solid phases (Figure 2. 5. (b)). The potential-pH diagram (Figure 2. 5. (a)) has the same restrictive conditions as the potential-pH diagrams shown in Figure 2. 3. (a). According to Figure 2. 5. (a), HSe^- would be the dominant aqueous species for all samples. To make Figure 2. 5. (b) reliable at 80 °C, log*K* values (Table 2. 4) are used as additional input in the thermodynamic database for Se reviewed and compiled by OECD/NEA. According to Figure 2. 5. (b), the experimental conditions fell into the stability field of $FeSe_2$(cr), which was identified by the XRD (Figure 2. 4).

The change in the Se concentrations with aging period is shown in Figure 2. 6. The Se concentrations gradually decreased with the increase in aging period. After 2 months and 3.5 months, the Se concentrations decreased to below the detection limit (DL) of the ICP-MS combined with USN (approximately 4×10^{-9} mol dm^{-3}). The DL values changed daily because of the variation in the analysis condition of the ICP-MS. There are two possible explanations for the measured decrease in Se concentrations. The first is that the experimental system was under a transitional condition which moved toward true equilibrium from over-saturation. The second is the rise of potential, which would decrease the solubility of Se(cr) and $FeSe_2$(cr).

If the experimental system was under a transitional condition which moved toward true equilibrium from over-saturation, the measured Se concentrations could be more than the calculated concentrations at 80 °C of the dissolution reaction of the solid phase which decreased the Se concentrations because the experiment was performed from over-saturation. To assess whether true equilibrium was attained or not and which solid phase controlled the Se concentrations, the measured Se concentrations were compared with the calculated concentrations at 80 °C of the dissolution reaction of Se(cr), FeSe(cr) and $FeSe_2$(cr) expressed by Equations (2-1), (2-2) and (2-3),

respectively:

$Se(cr) + H^+ + 2e^- \rightleftharpoons HSe^-$ log*K* at 80 °C = −7.19, (2-1)

$FeSe(cr) + H^+ \rightleftharpoons Fe^{2+} + HSe^-$ log*K* at 80 °C = −3.44, (2-2)

$FeSe_2(cr) + 2H^+ + 2e^- \rightleftharpoons Fe^{2+} + 2HSe^-$ log*K* at 80 °C = −15.88. (2-3)

The values of log*K* at 80 °C of Equations (2-1), (2-2) and (2-3) are based on the literature cited in Table 2. 4. The measured Se concentrations are plotted in Figure 2. 7. Because the Se concentrations after 2 months and 3.5 months decreased to below the detection limit (DL) of the ICP-MS, the arrows points extend to below the measured concentrations. The 3 sloped lines in Figure 2. 7 indicate the calculated HSe^- concentration using Equations (2-1), (2-2) and (2-3). Each sloped line in Figure 2. 7. (a), (b) and (c) corresponds to Equations (2-1), (2-2) and (2-3), respectively. The average of the measured Fe concentrations is used to draw the two sloped lines in Figure 2. 7. (b) and (c). Even if the highest or lowest Fe concentrations are used, the position of these two lines is less than 1 log unit different from the average of the measured Fe concentrations.

According to Figure 2. 7. (a), the Se concentrations after 1 month are lower than the calculated concentrations by the dissolution of Se(cr) as indicated by the sloped line. This means that Se(cr) did not control the Se concentrations after 1 month because this experiment was performed from over-saturation and the Se concentrations could not be lower than the calculated concentrations by the solid phase which controlled the Se concentrations. According to Figure 2. 7. (b), the measured concentrations were lower than the calculated concentrations by the dissolution of FeSe(cr) as indicated by the sloped line, with the only exception being for the measured concentrations at pH values of about 7. This means that FeSe(cr) also did not control the Se concentrations for the same reason as Se(cr), although it remains possible that FeSe(cr) controlled the Se concentrations after 1 month in the experiments with initial pH values of about 7.

According to Figure 2. 7. (c), the Se concentrations after 1 month are more than the calculated concentrations by the dissolution of $FeSe_2$(cr) as indicated by the sloped line. After 1 month, the experimental system was under a transitional condition which moved toward true equilibrium and the solid phase which decreased the Se concentrations was $FeSe_2$(cr).

After 2 months and 3.5 months, it is unclear whether true equilibrium was attained or not and which solid phase controlled the Se concentrations, because the Se concentrations decreased to below the DL of the ICP-MS. However, FeSe(cr) was an unlikely candidate of solubility limiting solid phase for Se because the Se concentrations after 2 month and 3.5 months fell below the calculated concentrations, as indicated by the sloped line in Figure 2. 7. (b).

After 1 month, despite the XRD patterns indicating that Se(cr) was the dominant solid phase (Figure 2. 4), Se(cr) did not control the Se concentrations. The experimental system was under a transitional condition, moving toward equilibrium from over-saturation, and the solid phase which decreased the Se concentrations was instead likely to be $FeSe_2$(cr), although it remains possible that FeSe(cr) controlled the Se concentrations in the experiments with initial pH values of about 7. After 2 months and 3.5 months, the transformation from Se(cr) to Fe-Se solid phase ($FeSe_2$(cr) and FeSe(cr)) was observed. Additionally, the experimental conditions constantly fell into the stability field of $FeSe_2$(cr) when plotted onto a potential-pH diagram using the available Se thermodynamic data, where the most stable solid phase is $FeSe_2$(cr) and the dominant aqueous specie is HSe^-. The formation of $FeSe_2$(cr) is likely to be caused in the long term by the presence of Fe resulting from carbon steel overpack corrosion in the engineered barrier systems under reducing conditions.

2.4 Conclusions

Two Se solubility experiments were performed in the presence of Fe under reducing conditions. The first used a bentonite (Kunigel V1®) equilibrated water and the second pure water.

In bentonite equilibrated waters, the experimental conditions fell into the stability field of $FeSe_2$(cr) when plotted on a potential-pH diagram, although no Se solid phases were identified.

Using pure water experiment, the experimental conditions constantly fell into the stability field of $FeSe_2$(cr) when plotted on a potential-pH diagram. After 1 month the experimental system was under a transitional condition, moving toward true equilibrium from over-saturation, and the solid phase which decreased the Se concentrations was likely to be $FeSe_2$(cr), although it remains possible that FeSe(cr) controlled the Se concentrations in the experiments with initial pH values of about 7. Se(cr) did not control the Se concentrations because the Se concentrations was lower than its solubility, even though the XRD patterns indicated that Se(cr) was the dominant solid phase.

After 2 months and 3.5 months, Se(cr) transformed to Fe-Se solid phase ($FeSe_2$(cr) and FeSe(cr)). The transformation from Se(cr) to Fe-Se solid phase ($FeSe_2$(cr) and FeSe(cr)) with the increase in aging period was observed by the XRD patterns. The formation of $FeSe_2$(cr) is likely to be caused in the long term by the presence of Fe, resulting from carbon steel overpack corrosion in the engineered barrier systems under reducing conditions.

References in Chapter 2.

1. Japan Nuclear Cycle Development Institute (JNC). H12: Project to establish the scientific and technical basis for HLW disposal in Japan - second progress report on research and development for the geological disposal of HLW in Japan. Japan: Japan Nuclear Cycle Development Institute; 2000.
2. Shibutani S, Yoshikawa H, Yui M. Solubility Measurement of Se in Se-H_2O System under Reducing Condition. PNC TN8410 94-204, Power Reactor and Nuclear Fuel Development Corporation; 1995 [in Japanese].
3. Yoshimura N. Clay Mineral and alteration action. The Association for the Geological Collaboration in Japan, Geoscience Libraries; 2001. No.32 p.215-216 [in Japanese].
4. Iida Y, Yamaguchi T, Tanaka T, Kitamura A, Nakayama S. Determination of Solubility Limiting Solid of Selenium in the Presence of Iron under Anoxic Conditions. Proc. Mobile Fission and Activation Products in Nuclear Waste Disposal; 2007 January 16-19; La Baule (France).
5. Andreas CS, Laurent C. [Selenite Reduction by Mackinawite, Magnetite and Siderite. XAS Characterization of Nanosized Redox Products]. Environ. Sci. Technol. 2008; 42:1984-1989.
6. Lee CP, Jan YL, Lan PL, Wei YY, Teng SP, Hsu CN. [Anaerobic and Aerobic Sorption of Cesium and Selenium on Mudrock]. J. Radioanal. Nucl. Chem. 2007; 274:145-151.
7. Doi R, Tachikawa H, Yui M. [Transformation of selenium solid phase in the presence of iron under reducing conditions]. J. Nucl. Sci. Technol. 2010; 47 No.3:278-285.

8. Olin Å, Noläng B, Öhman LO, Osadchii EG, Rosén E. Chemical thermodynamics of selenium. Amsterdam: ELSEVIER; 2005.
9. Wagman DD, Evans WH, Parker VB, Schumm RH, Halow I, Bailey SM, Churney KL, Nuttall RL. The NBS tables of chemical thermodynamic properties: selected values for inorganic and C_1 and C_2 organic substances in SI units. New York (NY): American Chemical Society and American Institute of Physics; 1982.
10. Robie RA, Hemingway BS, Thermodynamic Properties of Minerals and Related Substances at 298.15K and 1Bar (10^5 Pascals) Pressure and at Higher Temperatures. Washington: U.S. Geological Survey Bulletin 2131; 1995.
11. Mills KC, Thermodynamic Data for Inorganic Sulphides Selenides and Tellurides. London: London: Butterworths & Co (Publishers) Ltd; 1974.
12. Shock EL, Helgeson HC, Sverjensky DA. [Calculation of the Thermodynamic and Transport Properties of Aqueous Species at High Pressures and Temperatures: Standard Partial Molal Properties of Inorganic Neutral Species]. Geochim. Cosmochim. Acta, 1989; 53:2157-2183.

Tables and Figures in Chapter 2

Table 2. 1. Solution conditions of the bentonite equilibrated water and the water without bentonite

Solution	Bentonite equilibrated water	Water without bentonite
Initial Se concentration (mol dm^{-3})	1.0×10^{-3}	1.0×10^{-2}
Initial Fe concentration (mol dm^{-3})	1.0×10^{-3}	1.0×10^{-2}
Aging period (months)	1, 3	1, 2, 3.5
Temperature (°C)	60	80
Bentonite-liquid ratio (cm^3 g^{-1})	100	no bentonite

Table 2. 2. Chemical composition of the bentonite equilibrated water (mg kg^{-1} H_2O)

	Na	K	Ca	Mg	Fe	Al	SiO_2	Cl^-	NO_3^-	SO_4^{2-}	CO_3^{2-}
0.45 μm*	123	1.99	4.2	7.17	17.2	39.27	136.3	nm	nm	nm	nm
MWCO**	42.5	1.33	0.117	0.022	0.084	0.214	3.72	123	0.15	8.99	20.8

*: concentrations after passing through a membrane filter (pore size: 0.45μm)

**: concentrations after additionally passing through an ultra-fiter (MWCO:10,000)

nm = not measured

Table 2. 3. *E*, pH and Se concentrations of the bentonite equilibrated water

Sample No.	Aging period (month)	Initial pH	Initial *E** (mV)	Final pH	Final *E** (mV)	Final Se conc. (mol dm^{-3})
1-1	1	7.02	−228	6.99	−282	1.56×10^{-7}
1-2	1	7.04	−328	7.03	−277	1.94×10^{-8}
1-3	1	9.11	−323	9.06	−286	2.03×10^{-6}
1-4	1	9.11	−295	9.02	−283	1.63×10^{-6}
2-1	3	7.01	−233	7.24	−358	2.87×10^{-8}
2-2	3	7.00	−372	7.32	−365	1.94×10^{-8}
2-3	3	9.13	−288	9.21	−441	8.03×10^{-7}
2-4	3	9.08	−272	9.21	−448	7.37×10^{-7}

*：potential against the standard hydrogen electrode

Table 2. 4. Additional thermodynamic parameters used with the thermodynamic data for Se selected by OECD/NEA

Reaction	log$K$ at 60°C	log$K$ at 80°C	$\Delta_r H^0_m$ (kJ mol^{-1})	Reference
$SeO_3^{2-} = SeO_4^{2-}$* -0.5O_2(aq)**	13.340	12.538	-90.275	$\Delta_f G^0_m$ and $\Delta_f H^0_m$ of SeO_3^{2-}: [8]
$HSe^- = SeO_4^{2-}$* -2 O_2(aq)** +H^+	79.64	74.35	595.1	$\Delta_f G^0_m$ of HSe^-: [8] $\Delta_f H^0_m$ of HSe^- : [9]
H_2Se(aq) = SeO_4^{2-}* +2H^+ -2O_2(aq)**	75.816	70.546	-593.54	$\Delta_f G^0_m$ and $\Delta_f H^0_m$ of H_2Se : [8]
$HSeO_3^- = SeO_4^{2-}$* +H^+ -0.5O_2(aq)**	5.075	4.319	-85.11	$\Delta_f G^0_m$ and $\Delta_f H^0_m$ of $HSeO_3^-$: [8]
$HSeO_4^- = SeO_4^{2-}$* +H^+	-2.133	-2.318	-20.800	$\Delta_f G^0_m$ and $\Delta_f H^0_m$ of $HSeO_4^-$: [8]
H_2SeO_3(aq) = SeO_4^{2-}* +2H^+ -0.5 O_2(aq)	2.306	1.488	-92.12	$\Delta_f G^0_m$ and $\Delta_f H^0_m$ of H_2SeO_3(aq)$^-$: [8]
Se(cr) = SeO_4^{2-}* +2H^+ -1.5O_2(aq)** -H_2O*	34.422	31.763	-299.48	$\Delta_f G^0_m$ and $\Delta_f H^0_m$ of Se(cr): [8]
Se(mono) = SeO_4^{2-}* +2H^+ -1.5O_2(aq)** -H_2O*	34.647	31.988	-299.48	$\Delta_f G^0_m$ and $\Delta_f H^0_m$ of Se(mono): [8]
SeO_2(cr) = SeO_4^{2-}* +2H^+ -0.5O_2(aq)** -H_2O*	-0.001	-3.304	-372.05	$\Delta_f G^0_m$ and $\Delta_f H^0_m$ of SeO_2(cr): [8]
SeO_3(cr) = SeO_4^{2-}* +2H^+ -H_2O*	17.511	16.139	-154.570	$\Delta_f G^0_m$ and $\Delta_f H^0_m$ of SeO_3(cr): [8]
$FeSe_2$(cr) = 2SeO_4^{2-} * +2H^+ -3.5O_2(aq)** -H_2O* +Fe^{2+}	105.07	97.43	-861.1	$\Delta_f G^0_m$ and $\Delta_f H^0_m$ of $FeSe_2$(cr): [8] $\Delta_f G^0_m$ and $\Delta_f H^0_m$ of Fe^{2+} : [10]
FeSe(cr) = SeO_4^{2-}* -2O_2(aq)** +Fe^{2+}	76.27	70.91	-603.5	$\Delta_f G^0_m$ and $\Delta_f H^0_m$ of FeSe(cr) : [11] $\Delta_f G^0_m$ and $\Delta_f H^0_m$ of Fe^{2+} : [10]
Fe_2O_3 = -4H^+ +0.5O_2(aq)** +2H_2O* +2Fe^{2+}	-19.42	-18.83	66.3	$\Delta_f G^0_m$ and $\Delta_f H^0_m$ of Fe_2O_3 and Fe^{2+} : [10]
Fe_3O_4 = -6H^+ +0.5O_2(aq)** +3H_2O* +3Fe^{2+}	-12.78	-12.97	-21.2	$\Delta_f G^0_m$ and $\Delta_f H^0_m$ of Fe_3O_4 and Fe^{2+} : [10]
FeO(OH) = -2H^+ +0.25O_2(aq)** +1.5H_2O* +Fe^{2+}	-9.50	-9.15	39.7	$\Delta_f G^0_m$ and $\Delta_f H^0_m$ of FeO(OH) and Fe^{2+} : [10]

*：$\Delta_f G^0_m$ and $\Delta_f H^0_m$ of SeO_4^{2-} and H_2O are quoted from Olin et al. [8].

**：$\Delta_f H^0_m$ of O_2(aq) is quoted from Shock et al. [12].

Table 2. 5. *E*, pH and Se and Fe concentrations of the solutions used for the experiments in pure waters

Sample No.	Aging period (month)	Initial pH	Initial *E** (mV)	Final pH	Final *E** (mV)	Final Fe conc. (mol dm^{-3})	Final Se conc. (mol dm^{-3})
3-1	1	5.49	130	5.30	−257	9.90×10^{-3}	1.66×10^{-8}
3-2	1	4.89	121	5.31	−267	9.54×10^{-3}	1.22×10^{-8}
3-3	1	7.35	−94.0	6.97	−279	8.39×10^{-3}	1.08×10^{-8}
3-4	1	6.78	−96.0	7.01	−277	8.20×10^{-3}	1.10×10^{-8}
4-1	2	4.70	41.0	6.15	−186	8.99×10^{-3}	$<6.33\times10^{-9}$
4-2	2	5.60	136	6.17	−184	9.56×10^{-3}	$<6.33\times10^{-9}$
4-3	2	6.66	−83.0	6.25	−147	7.38×10^{-3}	$<6.33\times10^{-9}$
4-4	2	7.04	−10.2	6.31	−166	6.84×10^{-3}	$<6.33\times10^{-9}$
5-1	3.5	4.56	97.0	6.64	−190	9.49×10^{-3}	$<3.80\times10^{-9}$
5-2	3.5	5.10	130.0	6.40	−155	9.49×10^{-3}	$<3.80\times10^{-9}$
5-3	3.5	6.61	−98.0	6.33	−161	7.38×10^{-3}	$<3.80\times10^{-9}$
5-4	3.5	6.65	−80.0	6.33	−150	7.41×10^{-3}	$<3.80\times10^{-9}$

*：potential against the standard hydrogen electrode

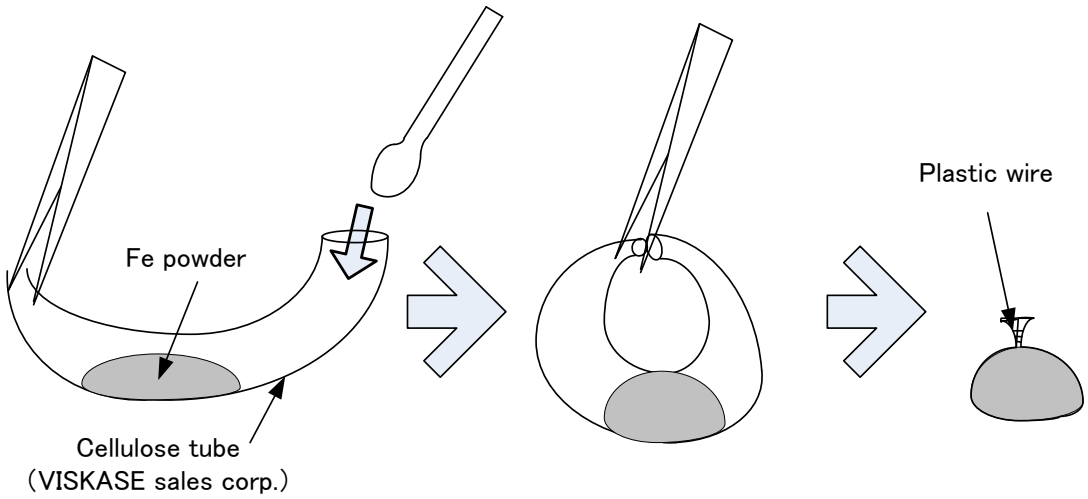

Figure 2. 1. Illustration of a cellulose tube tied on both sides by plastic wire used for the experiments in pure waters

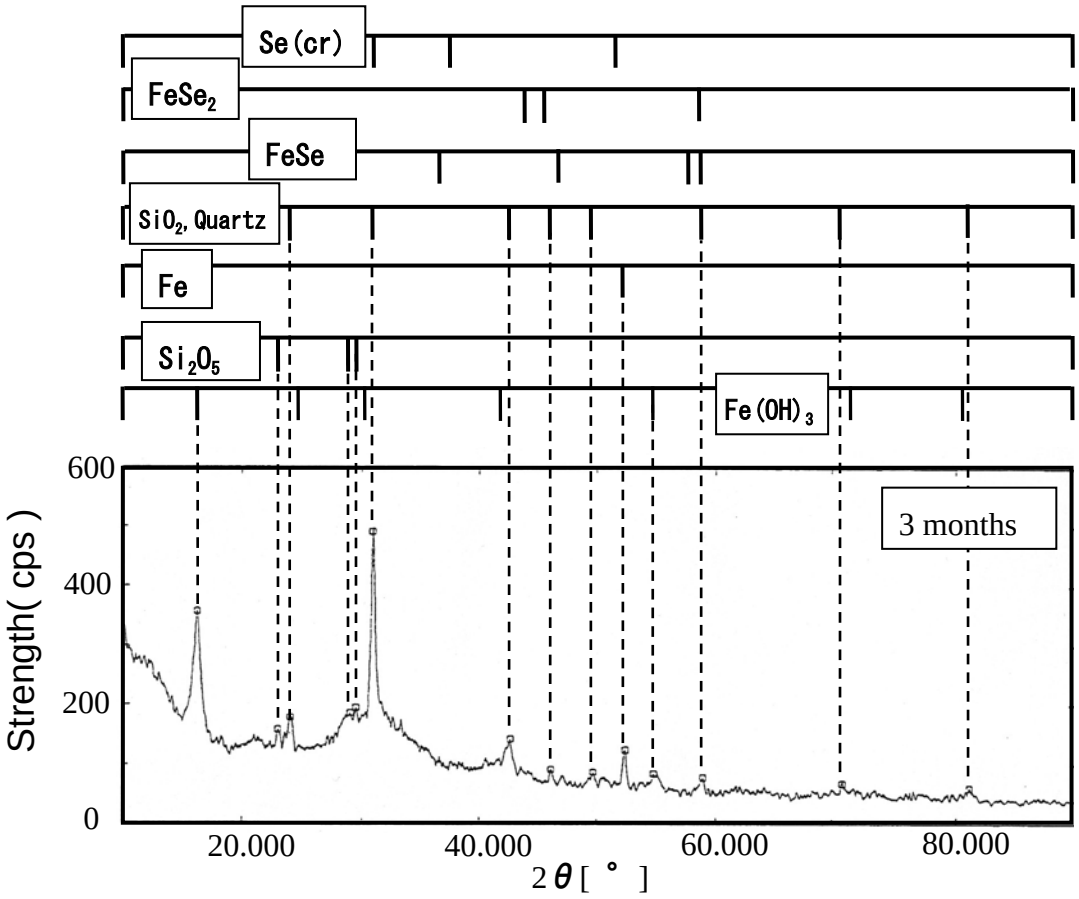

Figure 2. 2. XRD pattern of solid phase from the experiments in bentonite-equilibrated waters (initial pH = 7)

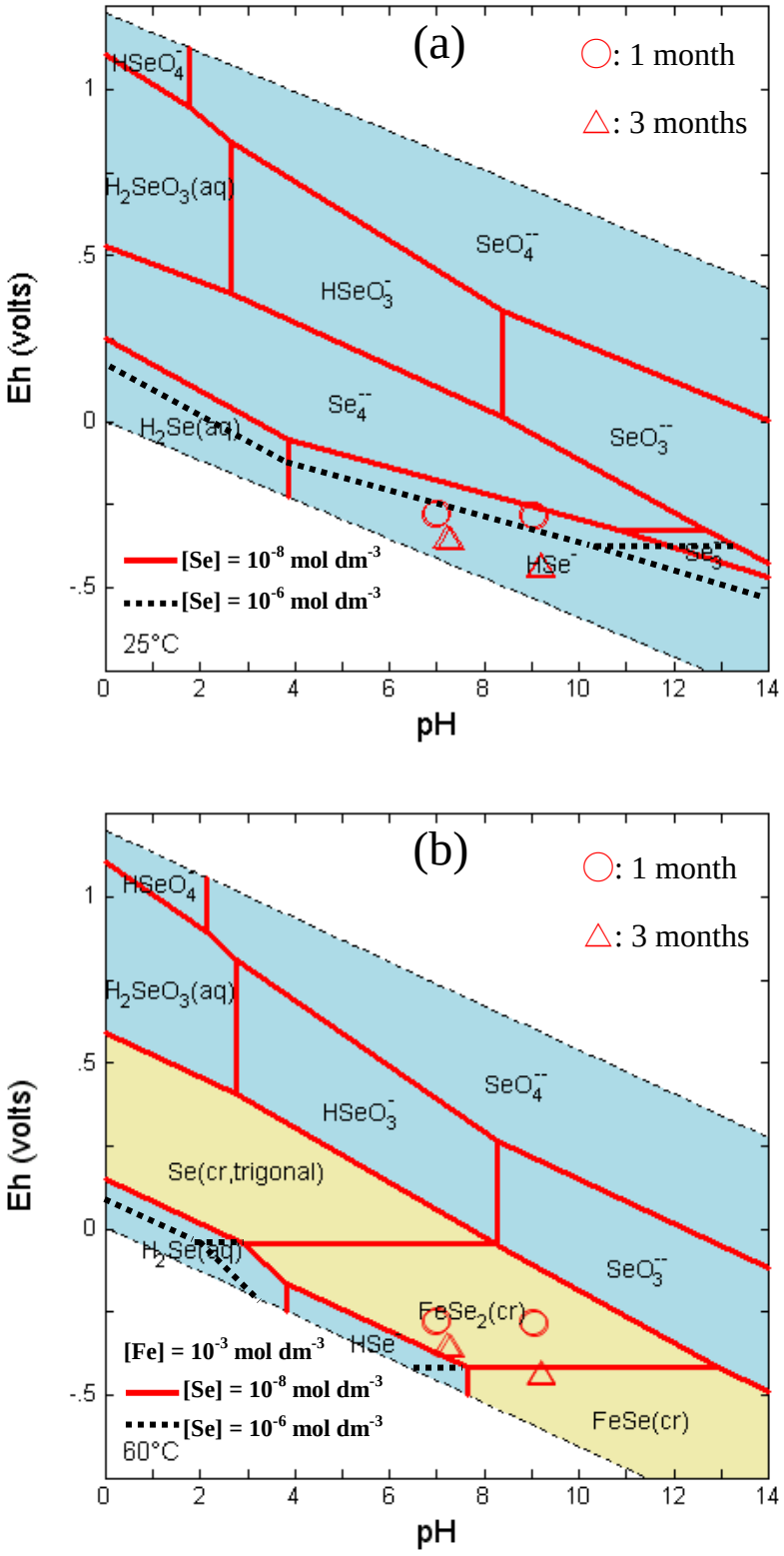

Figure 2. 3. Potential - pH diagram for the Se system showing the data points from the bentonite equilibrated water experiments. Potential - pH diagrams to identify the possible dominant aqueous species (a) and the stable solid phases (b). Eh is potential against the standard hydrogen electrode.

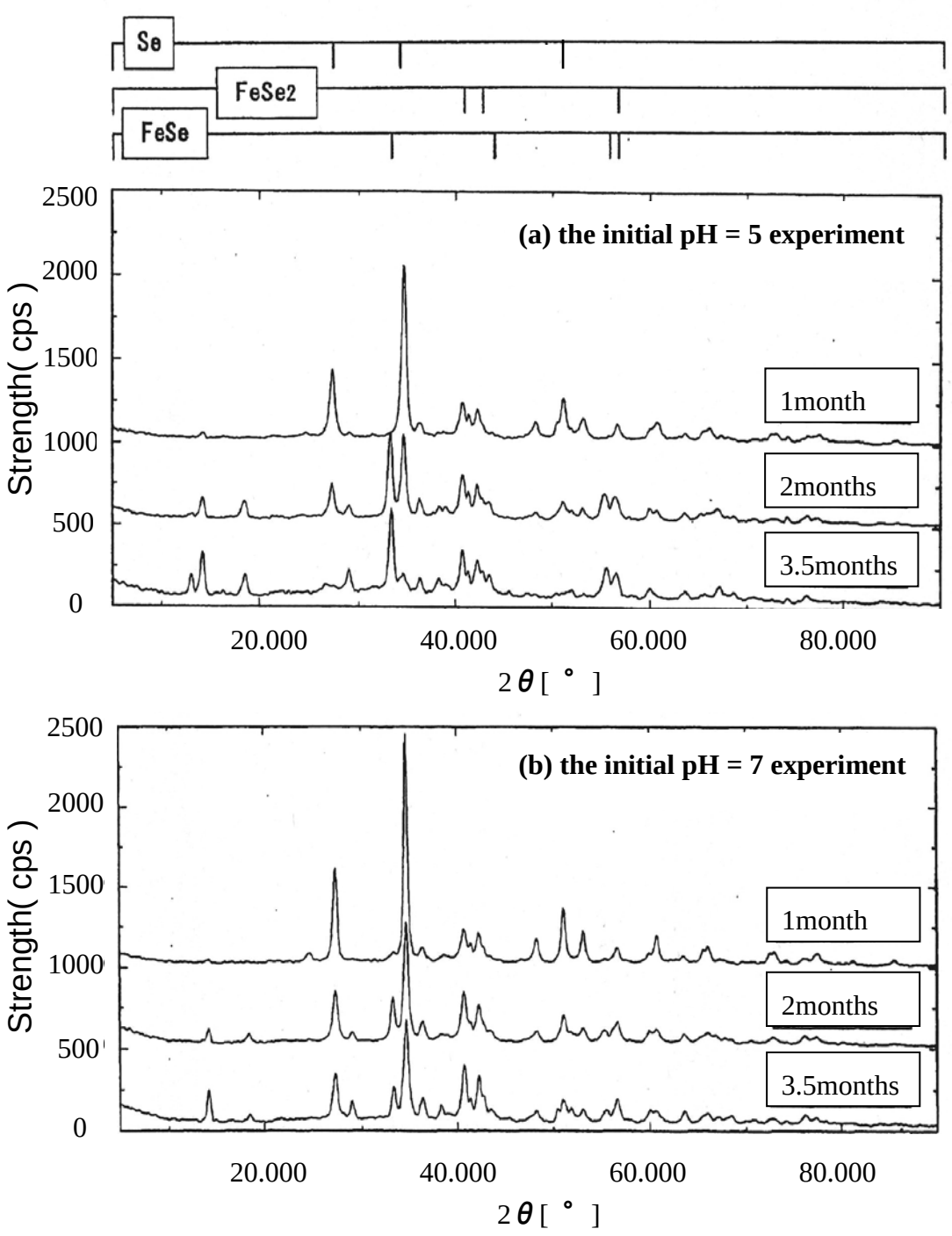

Figure 2. 4. XRD patterns of Se solid phases from the pure water experiments. XRD patterns from the initial pH = 5 experiment and the initial pH = 7 experiment are shown in (a) and (b), respectively.

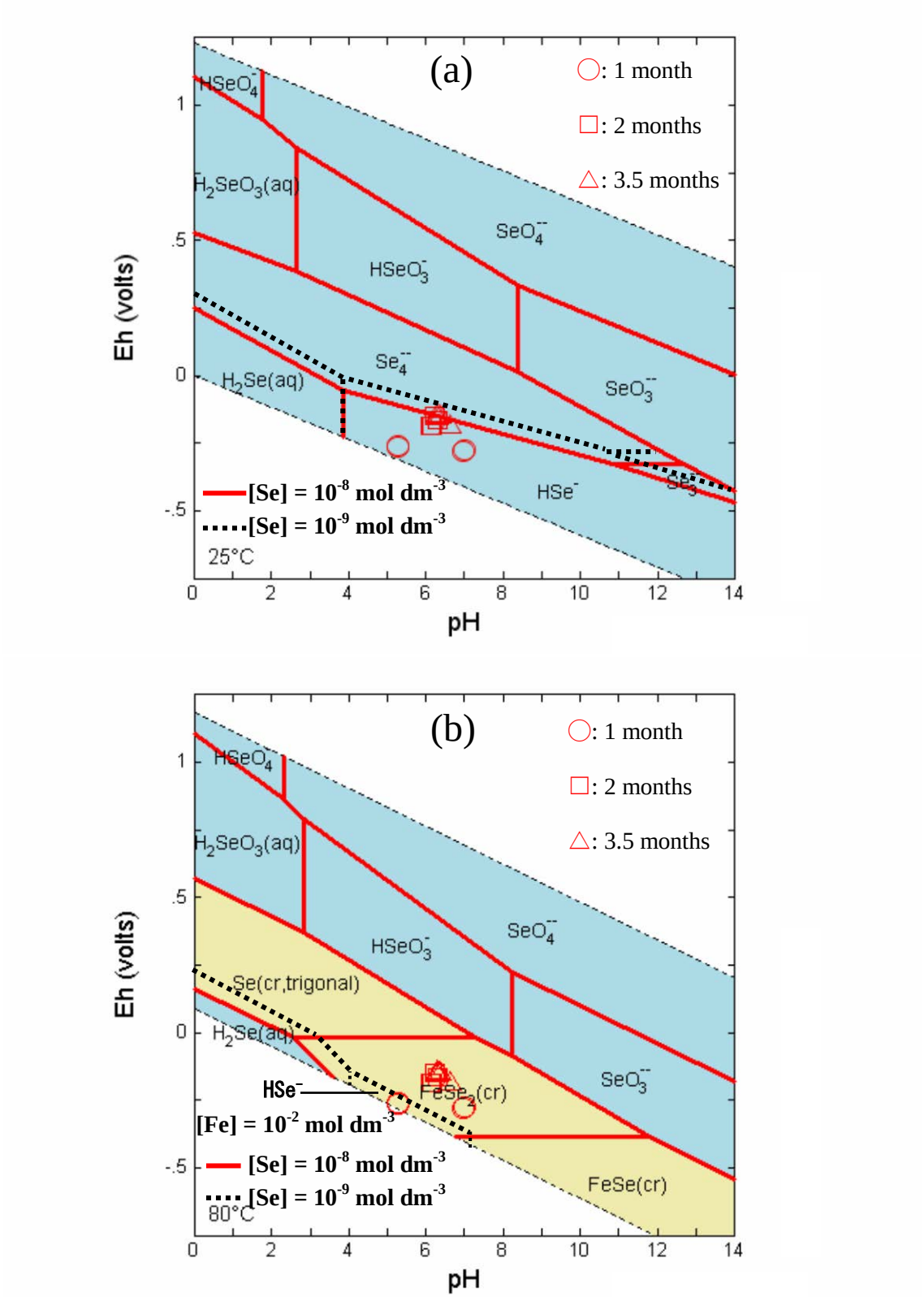

Figure 2. 5. Potential - pH diagram for Se system showing the data points from the pure water experiments. Potential - pH diagrams to identify the possible dominant aqueous species (a) and the stable solid phases (b). Eh is potential against the standard hydrogen electrode.

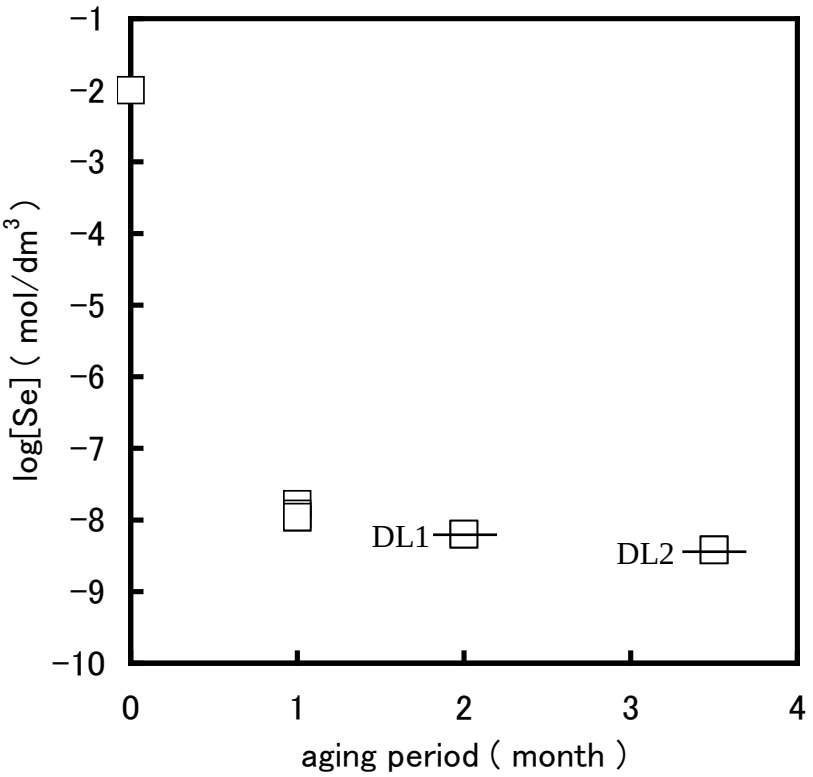

Figure 2. 6. Measured Se concentrations as a function of aging period from the pure water experiments. After 2 months and 3.5 months, Se concentrations fell below the detection limit (DL) of the ICP-MS. The DL values changed daily because of the variation in the analysis condition of the ICP-MS.

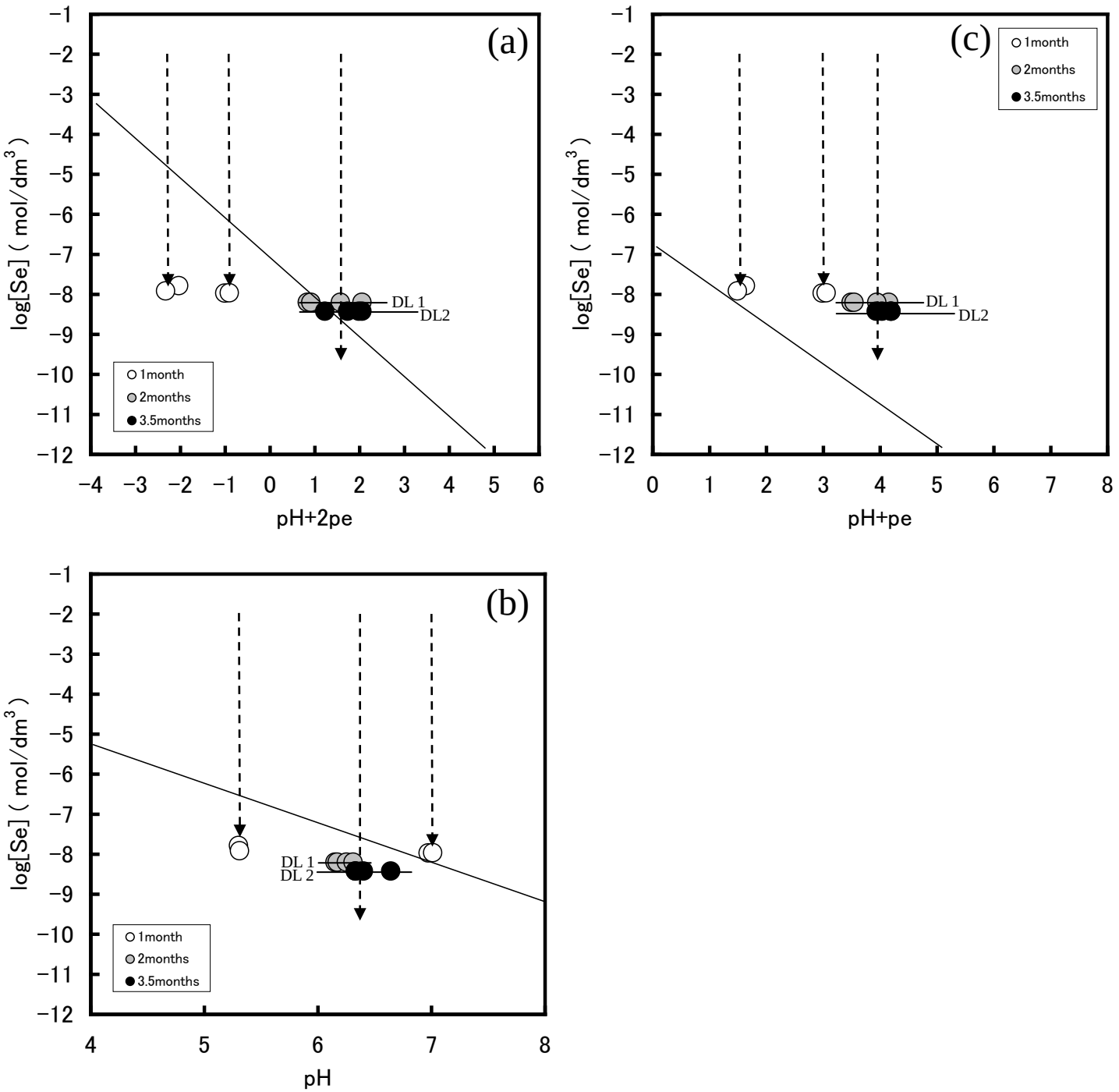

Figure 2. 7. Comparison of the measured Se concentrations (circles) with the calculated concentrations (sloped lines). Each sloped line in Figure 2. 7. (a), (b) and (c) corresponds to $Se(cr) + H^+ + 2e^- \rightleftharpoons HSe^-$ $\log K = -7.19$, $FeSe(cr) + H^+ \rightleftharpoons Fe^{2+} + HSe^-$ $\log K = -3.44$ and $FeSe_2(cr) + 2H^+ + 2e^- \rightleftharpoons Fe^{2+} + 2HSe^-$ $\log K = -15.88$, respectively. The top of the vertical dotted lines indicate the initial Se concentrations. Because the Se concentrations after 2 months and 3.5 months fell below the detection limit (DL) of the ICP-MS, the arrows points extends to below the measured concentrations. The average of the measured Fe concentrations is used to draw the two sloped lines in (b) and (c).

Chapter 3. Estimation of Se speciation in oxidized groundwater

3.1 Introduction

If the environmental conditions of repositories are oxidized due to decrease in the depth of repositories and/or the presence of oxidizing agents, the oxidation state of Se is changed to Se(IV) and/or Se(VI), and there is no Se solid phase controlling Se concentration because Se(IV) and Se(VI) are soluble. Increasing ionic strength decreased selenate (SeO_4^{2-}) sorption on amorphous iron oxide (am-$Fe(OH)_3$) and goethite (α-FeOOH) but did not affect selenite (SeO_3^{2-}) sorption [1]. Metallic iron and siderite ($FeCO_3$) reduced and immobilized Se(IV) and Se(VI) as iron diselenide ($FeSe_2$), the decrease in Se(IV) concentration was much greater than that in Se(VI) concentration under the same conditions [2]. Because the extent of sorption and immobilization of Se(IV) is different from that of Se(VI), the accurate prediction of Se(VI)-to-Se(IV) ratios is crucial for understanding the migration behavior of Se in those cases where the repositories exhibit oxidizing environments. An engineered barrier system will be constructed up to a depth of 300 m or more. If temperature is in the range of 40–50 °C at a depth of 500 m and the geothermal gradient is 3 °C /100 m [3], the decrease in the depth of repositories occurs at a temperature over 25 °C. Therefore, accurate prediction of Se(VI)-to-Se(IV) ratios is required for such a temperature. The Se(VI)/(IV) standard redox potential determines Se(VI)-to-Se(IV) ratios at 25 °C in thermodynamic models. Because the molar entropy of the reaction, $\Delta_r S^0{}_m$, yields the temperature derivatives of the standard redox potential, $\Delta_r S^0{}_m$ of the Se(VI)/(IV) couple is also required to predict the Se(VI)-to-Se(IV) ratios at a temperature over 25 °C. The accuracy of the prediction of Se(VI)-to-Se(IV) ratios using thermodynamic models hinges on that of the Se(VI)/(IV) standard redox potential and $\Delta_r S^0{}_m$ of the Se(VI)/(IV) couple.

Redox equilibrium between Se(IV) and Se(VI) have been little studied. This is apparently a consequence of slow reaction rates. For instance, it has been repeatedly demonstrated that the redox potential measured by a platinum electrode is not affected by Se(VI)-to-Se(IV) ratios in solution [4]. It is well known that selenic acid (H_2SeO_4) is prepared by oxidizing an aqueous solution of selenious acid (H_2SeO_3) with chlorine, and that H_2SeO_4 is reduced to H_2SeO_3 by treatment with concentrated hydrochloric acid. Sherrill and Izard [5] investigated the equilibrium conditions of the reaction represented as

$$Cl_2 + H_2SeO_3 + H_2O \rightleftharpoons 3H^+ + HSeO_4^- + 2Cl^- , \quad K = 1.42 \times 10^9 \qquad (3\text{-}1)$$

with the aid of the known chloride-chlorine standard redox potential for the purpose of determining the standard redox potential of the following reaction:

$$HSeO_4^- + 3H^+ + 2e^- \rightleftharpoons H_2SeO_3 + H_2O . \qquad (3\text{-}2)$$

To verify the equilibrium constant of Equation (3-1), Sherrill and Izard [5] investigated the corresponding oxidation-reduction reaction with bromine and hydrobromic acid in place of chlorine and hydrochloric acid:

$$Br_2 + H_2SeO_3 + H_2O \rightleftharpoons 3H^+ + HSeO_4^- + 2Br^- , \quad K = 0.88 . \qquad (3\text{-}3)$$

OECD/NEA has critically evaluated available thermodynamic data for Se [6]. The formation of the strong Se(IV) chloride complexes in solution of high hydrochloric acid concentration was reported by Milne and Lahaie [7] and Milne [8]. Olin et al. [6] did not select the equilibrium constant of Equation (3-1) because Sherrill and Izard [5] did not take into account Se(IV)-chloride complexation. On the other hand, Milne and Lahaie [9] reported that H_2SeO_3 was complexed by bromide as follows:

$$H_2SeO_3 + Br^- + H^+ \rightleftharpoons HSeO_2Br + H_2O , \quad K = 4.9 \pm 0.5 . \qquad (3\text{-}4)$$

Olin et al. [6] noted that the equilibrium constant of Equation (3-3) was determined without taking into account the existence of $HSeO_2Br$ although $HSeO_2Br$ was present under the

experimental conditions used in Sherrill and Izard [5]. However, using the equilibrium constant of Equation (3-3) without any corrections for side-reaction represented by Equation (3-4), Olin et al. [6] selected the following $HSeO_4^-/H_2SeO_3$ standard redox potential:

$E_{HSeO4\ -/H2SeO3}(T_0, 0) = 1.103 \pm 0.006$ V vs. SHE .

Olin et al. [6] also mentioned that more detailed discussion about the important Se(VI)/(IV) couple was required.

The Se(VI)/(IV) standard redox potential should be obtained from experiments performed in systems where no complex formations occur between Se species and the other species. In Doi and Yui [10, 11] and Doi [12], the determination of the Se(VI)/(IV) standard redox potential was performed in such a system using cyclic voltammetry, which is a typical method to measure the half-wave potential, $E_{1/2}(T, I_m)$. Even for the redox reaction whose rate is slow, cyclic voltammetry allows us to measure $E_{1/2}(T, I_m)$, which is the potential when the concentration of an oxidant is equal to that of a reductant. The following reactions were used to determine the Se(VI)/(IV) standard redox potential:

$SeO_4^{2-} + 3H^+ + 2e^- \rightleftharpoons HSeO_3^- + H_2O$, (see section 3.2) (3-5)

$SeO_4^{2-} + 2H^+ + 2e^- \rightleftharpoons SeO_3^{2-} + H_2O$. (see section 3.3) (3-6)

The Se(VI)/(IV) half-wave potentials were measured by cyclic voltammetry experiments as a function of the molality of a sodium ion, m_{Na+}. Extrapolation of the experimental data to $m_{Na+} = 0$ using SIT [13] yields the Se(VI)/(IV) standard redox potential. Finally, the consistency between $E_{SeO4\ 2-/HSeO3\ -}(T, 0)$ determined by Doi and Yui [10, 11], $E_{SeO4\ 2-/SeO3\ 2-}(T, 0)$ determined by Doi [12] and the corrected value of the equilibrium constant of Equation (3-3) was verified.

No existing experimental studies report the value for $\Delta_r S^0{}_m$ of the Se(VI)/(IV) couple, which results in the poor prediction of Se(VI)/Se(IV) ratios at a temperature over 25°C.

Therefore, the objective of Doi [14] is to obtain $\Delta_r S^0_m$ of the Se(VI)/(IV) couple from the temperature dependence of the Se(VI)/(IV) standard redox potential.

Because no experimental data were available at that time, Olin et al. [6] estimated $\varepsilon_T(i, j)$ for Se species using an analogy with sulfur (S). The uncertainty in $\varepsilon_T(i, j)$ for Se species estimated by Olin et al. [6] was the same as that in $\varepsilon_T(i, j)$ for the similar S species. However, after that, Philippini et al. [15] experimentally determined $\varepsilon_T(i, j)$ for Se species and reported differences between $\varepsilon_T(i, j)$ for Se species and S species. Based on this experimental investigation, the applicability of an analogy with S to estimate $\varepsilon_T(i, j)$ for Se species is questionable. Therefore it is necessary to determine $\varepsilon_T(i, j)$ for Se species by experimental investigations. Previous reports [10, 11, 12, 16, 17] determined the stoichiometric sum of $\varepsilon_T(i, j)$, $\Delta\varepsilon_T(i, j)$, instead of $\varepsilon_T(i, j)$. This was because $\varepsilon_T(i, j)$ for both an oxidant and a reductant had to be considered when $E_{1/2}(T, I_m)$ determined experimentally at different ionic strengths were corrected by extrapolating to zero ionic strength to obtain the standard redox potential. If either an oxidant or a reductant is an uncharged species, then $\varepsilon_T(i, j)$ for the other species can be determined because $\varepsilon_T(i, j)$ for uncharged species is zero [6]. To obtain the value for $\varepsilon_{T0}(HSeO_4^-, Na^+)$, the following reaction involving $HSeO_4^-$ as the oxidant and the uncharged species (H_2SeO_3) as the reductant was used in Doi [14]:

$$HSeO_4^- + 3H^+ + 2e^- \rightleftharpoons H_2SeO_3 + H_2O \ . \qquad (3\text{-}7)$$

In spite of the fact that the pH of groundwater is anticipated to be 7 to 9 [3], the reactions occurring in an acidic solution (Equation (3-5) and Equation (3-7)), and that occuring in an alkaline solution (Equation (3-6)) were used in Chapter 3. The standard thermodynamic data for the protonation reactions for Se species are available [6]. Because the Se speciation is calculated using a thermodynamic database including the standard thermodynamic data for the protonation reactions for Se species, it is possible to calculate the Se speciation at the

anticipated pH of groundwater even though the standard thermodynamic data of the Se(VI)/(IV) couple included in a thermodynamic database are not those of the reaction occurring at such a pH. Because Chapter 3 assigned a priority to the determination of the standard thermodynamic data of the Se(VI)/(IV) couple and $\varepsilon_T(i, j)$ for the Se species, the thermodynamic values for the reactions not occurring in weakly alkaline repository groundwaters were evalulated for each purpose.

3.2 Determination of the standard redox potential of the $SeO_4^{2-}/HSeO_3^-$ couple

3.2.1 Experimental

Cyclic voltammograms were obtained by using an electrochemical analyzer (BAS Inc., ALS Model 1100). A three-electrode system was employed. Doi and Yui [10] used the glass cell (BAS Co., Ltd., 001056) composed of a circuit with a platinum working electrode (ALS, No. JA018Pt) with an exposed area of 3.1 mm^2, a platinum counter-electrode (ALS, No. 002233 VC-3 5cmPt) and a saturated calomel reference electrode with a saturated solution of KCl (ALS, No. 002056 RE-2B). The working electrode was polished using a 0.05μm alumina paste before each cyclic voltammetry experiment.

A solution of Se at a concentration of 1.00×10^{-4} mol dm^{-3} was prepared by the addition of Se standard solution (994 mg dm^{-3} Se in 0.10 mol dm^{-3} HNO_3, Kanto Chemical Co., Inc.) and sodium perchlorate monohydrate ($NaClO_4 \cdot H_2O$, Kishida Chemical Company) into the deionized water. All reagents were used without further purification. The molality of Na^+, m_{Na+}, was adjusted to 0.500, 1.00, 1.50 and 2.00 mol kg^{-1}. Before each cyclic voltammetry experiment, pH values were measured using the combination glass pH electrode (TOA Co., Ltd., ION METER HM-60V). The observed pH (pH_{obs}) were within the range of $pH_{obs} = 3.0 \pm 0.2$. The solution not containing Se (henceforth referred to as the “blank” solution) was prepared using HNO_3 ($[HNO_3] = 8 \times 10^{-4}$ mol dm^{-3}). Aliquots of solution were transferred to the glass cell. To fulfill the oxygen-free condition, all solutions were thoroughly degassed with nitrogen gas prior to recording cyclic voltammograms. The cyclic voltammetry experiments were performed at room temperature. The scan rate was 0.1 V s^{-1}. The scan region was 0.000 ↔ 1.200 V vs. SCE, which corresponds to 0.241 ↔ 1.441 V vs. SHE, described as a vertical dotted line in Figure 3. 1.

3.2.2 Data analysis

When that redox process is reversible or quasi-reversible, $E_{1/2}(T, I_m)$ is the potential when the concentration of a reductant, [*Red*], is equal to that of an oxidant, [*Ox*] [16]. Nernst's equation for the redox reaction, $Ox + pH^+ + ne^- = Red + qH_2O$, is

$$E = E_{Ox/Red}(T, 0) + \frac{RT}{nF} \ln \frac{a_{Ox} a_{H+}^{p}}{a_{Red} a_{H2O}^{q}} = E_{1/2}(T, I_m) + E_{Ref}(T, I_{Ref}) + \frac{RT}{nF} \ln \frac{[Ox]}{[Red]} . \quad (3\text{-}8)$$

The following relationship between $E_{1/2}(T, I_m)$ and $E_{Ox/Red}(T, 0)$ can be obtained from Equation (3-8):

$$E_{1/2}(T, I_m) + E_{Ref}(T, I_{Ref}) = E_{Ox/Red}(T, 0) + (RT/nF \log e)(\log \gamma_{Ox} - \log \gamma_{Red} + p \log a_{H+} - q \log a_{H2O}). \quad (3\text{-}9)$$

SIT [13] gives a good estimate of activity coefficient, γ_i, in an ionic medium of up to 3.5 mol kg^{-1}. SIT was used to calculate $\log \gamma_{Ox}$ and $\log \gamma_{Red}$ because the highest ionic strength was less than 3 mol kg^{-1} in Doi and Yui [10]. The activity coefficient γ_i of ion i with charge z_i is described by

$$\log \gamma_i = - z_i^2 D(T, I_m) + \sum_j \varepsilon_T (i, j) m_j , \quad (3\text{-}10)$$

where

$$D(T, I_m) = A(T) I_m^{1/2} / (1 + b_j B(T) I_m^{1/2}), \quad (3\text{-}11)$$

and the summation extends over all ions j of opposite charge of i. $D(T, I_m)$ is the Debye-Hückel term [13]. $A(T)$ and $B(T)$ are temperature dependent constants and b_j is an ion size parameter for the hydrated ion j. The values of $A(T)$ and $B(T)$ are taken from Olin et al. [6]. The cyclic voltammetry experiments were performed at a temperature in the range of 20.7−25.0 °C. For such a temperature range, Doi and Yui [10, 11] took into account the temperature dependence of $D(T, I_m)$. $D(20℃, I_m)$ was calculated from A(20°C) and B(20°C) and D(25°C, I_m) from A(25°C) and B(25°C). As decribed later, both D(20°C, I_m) and D(25°C, I_m) were used. From $b_j B(T_0) = 1.5$ $kg^{1/2}$ $mol^{-1/2}$ and $B(T_0) = 3.284 \times 10^9$ $kg^{1/2}$ $mol^{-1/2}$ m^{-1} [6],

b_j is calculated to be 4.568×10^{-10} m at 25 °C. With the assumption that b_j is independent of temperature [18], the b_j value at 25 °C was used when $D(20℃, I_m)$ was calculated using Equation (3-11). Cations that should be considered were Na^+ in a solution of Se. In case that Se exists as anion i, $\log\gamma_i$ is described by

$$\log \gamma_i = - z_i^2 D(T, I_m) + \varepsilon_T(i, Na^+) m_{Na+}. \quad (3\text{-}12)$$

The temperature dependence of $\varepsilon_T(i, j)$ and $E_{Ref}(T, I_{Ref})$ was neglected for the temperature range of 20.7−25.0 °C. For the $SeO_4^{2-}/HSeO_3^-$ couple, the following relationship was obtained by substituting Equation (3-12) for the activity coefficients in Equation (3-9):

$$E_{1/2}(T, I_m) + E_{Ref}(T_0, I_{Ref}) = E_{SeO4\ 2-/HSeO3\ -}(T_0, 0) + J\{-3D(T, I_m) + \Delta\varepsilon_1 m_{Na+} + 3\log a_{H+} - \log a_{H2O}\} \quad (3\text{-}13)$$

where $J = RT/2F\log e$, $\Delta\varepsilon_1 = \varepsilon_{T0}(SeO_4^{2-}, Na^+) - \varepsilon_{T0}(HSeO_3^-, Na^+)$ and $E_{Ref}(T_0, I_{Ref}) = 0.241$ V vs. SHE in case of the saturated calomel reference electrode with a saturated solution of potassium chloride (KCl). Consequently, the following equation is obtained:

$$Y_1 = \Delta\varepsilon_1 m_{Na+} + E_{SeO4\ 2-/HSeO3\ -}(T_0, 0)/J, \quad (3\text{-}14)$$

where

$$Y_1 = \{E_{1/2}(T, I_m) + E_{Ref}(T_0, I_{Ref})\}/J + 3D(T, I_m) - 3\log a_{H+} + \log a_{H2O}. \quad (3\text{-}15)$$

The values of Y_1 are plotted vs. m_{Na+}. As one would predict from Equation (3-14), the extrapolation of Y_1 to $m_{Na+} = 0$ gives a straight line where the slope and intercept correspond to $\Delta\varepsilon_1$ and $E_{SeO4\ 2-/HSeO3\ -}(T_0, 0)/J$, respectively.

Y_1 are calculated using Equation (3-15). $E_{1/2}(T, I_m)$ was measured by the cyclic voltammetry experiment. The value of pH_{obs} was directly used as a substitute for $-\log a_{H+}$. The values of $\log a_{H2O}$ are calculated by

$$\log a_{H2O} = \frac{-\phi \sum_k m_k}{55.51 \times \ln 10} \quad (3\text{-}16)$$

where ϕ is the osmotic coefficient of the mixture and the summation extends over all solute species k with molality m_k present in the solution [6]. In the presence of a supporting electrolyte $NaClO_4$ of a concentration much higher than those of the reacting ions, the osmotic coefficient can be calculated by

$$1-\phi = \frac{A(T)\ln 10\left|z_{Na^+} z_{ClO_4^-}\right|}{(1.5)^3 I_m}\left[1+1.5\sqrt{I_m}-2\ln(1+1.5\sqrt{I_m})-\frac{1}{1+1.5\sqrt{I_m}}\right]$$

$$- (0.5\ln 10)\,\varepsilon_{T0}(Na^+, ClO_4^-) m_{NaClO4}, \qquad (3\text{-}17)$$

where $\varepsilon_{T0}(Na^+, ClO_4^-) = 0.01 \pm 0.01$ [13]. As mentioned earlier, both $D(20°C, I_m)$ and $D(25°C, I_m)$ were calculated using Equation (3-11). $Y_1(20°C)$ and $Y_1(25°C)$ was calculated from $D(20°C, I_m)$ and $D(25°C, I_m)$, respectively.

3.2.3 Results and discussion

Figure 3. 2 shows the cyclic voltammogram of the blank solution. A small peak at about 1.0 V vs. SHE and that at about 0.5 V vs. SHE are attributed to the formation of an oxide film on the electrode surface and to the corresponding reduction of the oxide film, respectively. No voltammetric peaks associated with the oxidation-reduction reaction of HNO_3 are observed.

Figure 3. 3 shows the cyclic voltammogram of a solution containing Se after repetitive potential cycling. With increasing number of cycles, both the anodic and cathodic peaks appear clearly. The sharp drop of the anodic current at the upper reversal potential, observed during the course of first few cycles, suggests a considerable decrease in the active electrode area available for the electron-transfer process, owing to the formation of a passivating layer covering the electrode surface. The growth of the redox wave is indicative of the increase in the active electrode area owing to the removal of this passivating layer by repetitive potential

cycling. The cyclic voltammogram becomes steady by the 20th cycle. The complete removal of this passivating layer results in a steady voltammogram. The $E_{1/2}(T, I_m)$ value was obtained from the 27th cyclic voltammogram.

The assignment of the voltammetric peaks requires the experimental verification of the dependence of the peak current on the scan rate, *v*. The linear dependence of the peak current on $v^{1/2}$ is evidence of a diffusion-controlled process [19, 20]. Although Doi and Yui [10] did not verify the dependence of the peak current on *v*, they assumed that the anodic peak and the cathodic peak were diffusion-controlled processes. With this assumption, the peak at about 1.2 V vs. SHE and that at about 0.5 V vs. SHE were attributed to the oxidation of $HSeO_3^-$ to SeO_4^{2-} and to the corresponding reduction of SeO_4^{2-} to $HSeO_3^-$, respectively.

As described in section 3.2.2, Equation (3-9) can be used in case that the redox process is reversible or quasi-reversible. The reversibility of the redox process can be confirmed by the experimental verification of the dependence of the peak potential on *v*. However, without this verification, Doi and Yui [10] assumed that the redox process was reversible. This was because the absolute value of the anodic peak current was equal to that of the cathodic peak current, in other words, the cyclic voltammogram was symmetric shape. With this assumption, Equation (3-9) was used to determine $E_{SeO4\ 2-/HSeO3\ -}(T_0, 0)$. To obtain evidence of a reversible process, the dependence of the peak potential on *v* needs to be verified.

The $E_{1/2}(T, I_m)$ values measured in acidic sodium perchlorate solutions as a function of m_{Na+} are listed in Table 3.1. A plot of Y_1(20°C) vs. m_{Na+} and that of Y_1(25°C) vs. m_{Na+} are shown in Figure 3. 4 and in Figure 3. 5, respectively. The value of $E_{SeO4\ 2-/HSeO3\ -}(T_0, 0)$ is obtained by using the extrapolation of weighted linear regression [21] through Y_1 determined at various m_{Na+}, which corresponds to the line shown in Figure 3. 4 and that shown in Figure

3. 5. The intercept of the line shown in Figure 3. 4 corresponds to $E_{\mathrm{SeO4\ 2-/HSeO3\ -}}(T_0, 0)$ given by

$E_{\mathrm{SeO4\ 2-/HSeO3\ -}}(T_0, 0) = 1.064 \pm 0.001$ V vs. SHE.

The intercept of the line shown in Figure 3. 5 corresponds to $E_{\mathrm{SeO4\ 2-/HSeO3\ -}}(T_0, 0)$ given by

$E_{\mathrm{SeO4\ 2-/HSeO3\ -}}(T_0, 0) = 1.083 \pm 0.001$ V vs. SHE.

Doi and Yui [10, 11] finally reported the following value, which covers the above two values:

$E_{\mathrm{SeO4\ 2-/HSeO3\ -}}(T_0, 0) = 1.074 \pm 0.011$ V vs. SHE.

The determination process of $E_{\mathrm{SeO4\ 2-/HSeO3\ -}}(T_0, 0)$ involved some problems. Although it was assumed that the tetravalent Se species was only $HSeO_3^-$ in the bulk solution, $HSeO_3^-$ and H_2SeO_3(aq) could coexist because the experimental condition of $pH_{obs} = 3.0 \pm 0.2$ was near the boundary between these two species in a potential-pH diagram (Figure 3. 1). Therefore, in order to prevent the proton addition to the reductant, Doi [12] used high pH solution, in which the tetravalent Se species was only SeO_3^{2-}.

The value of pH_{obs} was directly used to determine $E_{\mathrm{SeO4\ 2-/HSeO3\ -}}(T_0, 0)$ in spite of the fact that pH_{obs} might be different from $-\log a_{H+}$ because of the difference between the activity factor of the calibration buffer and high ionic strength solution. The reliable determination of the Se(VI)/(IV) standard redox potential requires the accurate value of $-\log a_{H+}$. Therefore, instead of pH_{obs}, the pH value corresponding to $-\log a_{H+}$ was calculated using SIT in Doi [12] and Doi [14] (see section 3.3.2 and section 3.4.2).

Because the temperature was not controlled, Doi and Yui [10, 11] used both D(20°C, I_m) and D(25°C, I_m) in the process of determining $E_{\mathrm{SeO4\ 2-/HSeO3\ -}}(T_0, 0)$, which resulted in increase in the uncertainty in $E_{\mathrm{SeO4\ 2-/HSeO3\ -}}(T_0, 0)$. Therefore, the temperature of the solution in the cell was controlled in Doi [12] and Doi [14].

As mentioned above, the experimental verification of the dependence of the peak

current on v is necessary to obtain evidence of a diffusion-controlled process. The experimental verification of the dependence of the peak potential on v is also necessary to confirm the reversibility of the redox process. A further investigation of Se, using cyclic voltammetry, has been carried out for the purpose of clarifying the remaining issues and determining the more reliable Se(VI)/(IV) standard redox potential [12]. See section 3.3.

3.2.4 Conclusions

An electrochemical investigation, using cyclic voltammetry, has been carried out to determine the standard redox potential of the following redox reaction:

$$SeO_4^{2-} + 3H^+ + 2e^- \rightleftharpoons HSeO_3^- + H_2O \ .$$

The Se(VI)/(IV) half-wave potentials were measured in acidic sodium perchlorate solutions as a fuction of m_{Na+}. Extrapolation of the experimental data to $m_{Na+} = 0$ using SIT yields the following standard redox potential:

$$E_{SeO4\ 2-/HSeO3\ -}(T_0, 0) = 1.074 \pm 0.011 \text{ V vs. SHE.}$$

3.3 Determination of the standard redox potential of the SeO_4^{2-}/SeO_3^{2-} couple

3.3.1 Experimental

Doi [12] used the alkaline-resistant Teflon cell (Interchem Co., Ltd., Tefloncell250) composed of a circuit with a platinum working electrode (Interchem Co., Ltd., PtWE) with an exposed area of 3.1 mm^2, a platinum counter-electrode (Interchem Co., Ltd., PtCE) and an alkaline-resistant Hg/HgO reference electrode with a 1 mol dm^{-3} solution of sodium hydroxide (NaOH) (Interchem Co., Ltd., Alkali). The working electrode was polished using a 0.05μm alumina paste before each cyclic voltammetry experiment.

A solution of Se at a concentration of 6.6×10^{-3} mol kg^{-1} was prepared by the addition of selenious acid (H_2SeO_3) and $NaClO_4$ into 0.1 mol dm^{-3} NaOH. All reagents were purchased from Kanto Chemical Co., Inc. and used without further purification. The molality of Na^+ was adjusted to 0.10, 0.48, 0.96 and 1.45 mol kg^{-1}. The tetravalent Se species was SeO_3^{2-} because the values of $-\log a_{H+}$ were estimated to be 12.68 ± 0.05 as described in section 3.3.2. The blank solution was prepared using $NaClO_4$ and NaOH ($-\log a_{H+}$ = 12.90 ± 0.02, m_{Na+} = 1.44 mol kg^{-1}). Aliquots of solution were transferred to the alkaline-resistant Teflon cell. For all the cyclic voltammetry experiments, the temperature of the solution in the Teflon cell was maintained at 25.0 ± 0.5 °C by the thermostat water bath (AS ONE Co., Ltd., Thermax TM-1). All solutions were thoroughly degassed with nitrogen gas prior to recording cyclic voltammograms. The scan rate was 0.1 V s^{-1} except while investigating the dependence of the peak current and potential on *v*. The scan region was −0.398 ↔ 0.501 V vs. Hg/HgO, which corresponds to −0.293 ↔ 0.606 V vs. SHE, described as a line with arrow points in Figure 3. 1.

3.3.2 Data analysis

The temperature of a solution of Se was maintained at 25.0 ± 0.5 °C, which resulted in $T = T_0$. For the SeO_4^{2-}/SeO_3^{2-} couple, the following relationship was obtained by substituting Equation (3-12) for the activity coefficients in Equation (3-9):

$$E_{1/2}(T_0, I_m) + E_{\mathrm{Ref}}(T_0, I_{\mathrm{Ref}}) = E_{\mathrm{SeO4\ 2-/SeO3\ 2-}}(T_0, 0) + J(\Delta\varepsilon_2 m_{\mathrm{Na+}} + 2\log a_{\mathrm{H+}} - \log a_{\mathrm{H2O}}), \quad (3\text{-}18)$$

where $\Delta\varepsilon_2 = \varepsilon_{T0}(SeO_4^{2-}, Na^+) - \varepsilon_{T0}(SeO_3^{2-}, Na^+)$ and $E_{\mathrm{Ref}}(T_0, I_{\mathrm{Ref}}) = 0.105$ V vs. SHE (calculated using SIT) in case of the Hg/HgO reference electrode in a solution of 1 mol dm^{-3} NaOH. Consequently, the following equation is obtained:

$$Y_2 = \Delta\varepsilon_2\, m_{\mathrm{Na+}} + E_{\mathrm{SeO4\ 2-/SeO3\ 2-}}(T_0, 0)/J, \quad (3\text{-}19)$$

where

$$Y_2 = \{E_{1/2}(T_0, I_m) + E_{\mathrm{Ref}}(T_0, I_{\mathrm{Ref}})\}/J - 2\log a_{\mathrm{H+}} + \log a_{\mathrm{H2O}}. \quad (3\text{-}20)$$

The values of Y_2 are plotted vs. $m_{\mathrm{Na+}}$. As one would predict from Equation (3-19), the extrapolation of Y_2 to $m_{\mathrm{Na+}} = 0$ gives a straight line where the slope and intercept correspond to $\Delta\varepsilon_2$ and $E_{\mathrm{SeO4\ 2-/SeO3\ 2-}}(T_0, 0)/J$, respectively.

Y_2 are calculated using Equation (3-20). $E_{1/2}(T_0, I_m)$ was measured by the cyclic voltammetry experiment. Instead of pH_{obs}, the pH value corresponding to the activity of H^+ is predicted using the following equation:

$$\mathrm{pH} = -\log a_{\mathrm{H+}} = -\log K_{\mathrm{w}} + \log[\mathrm{OH^-}] + \log\gamma_{\mathrm{OH-}} - \log a_{\mathrm{H2O}}, \quad (3\text{-}21)$$

where K_w was the ionic product of water (1.01×10^{-14}) [22]. Using SIT, $\log\gamma_{OH-}$ is calculated by

$$\log\gamma_{\mathrm{OH-}} = -D(T_0, I_m) + \varepsilon_{T0}(\mathrm{Na^+}, \mathrm{OH^-})m_{\mathrm{Na+}}, \quad (3\text{-}22)$$

where $\varepsilon_{T0}(Na^+, OH^-) = 0.04 \pm 0.01$ kg mol^{-1} [13]. Using Equation (3-11), the value of $D(T_0, I_m)$ was calculated from $A(T_0)$ and $b_j B(T_0)$ taken from Olin et al. [6]. The value of $\log a_{H2O}$

was calculated using Equation (3-16). The osmotic coefficient for a mixed electrolyte can be calculated using the following equations:

$$\phi - 1 = \left(\sum_i m_i \right)^{-1} \left\{ 2 I_m f^{\phi} + 2 \sum_c \sum_a m_c m_a \left[B_{ca}^{\phi} + \frac{\left(\sum mz \right)}{\left(z_c z_a \right)^{1/2}} C_{ca}^{\phi} \right] \right\}, \quad (3\text{-}23)$$

$$f^{\phi} = -0.392 \left[\sqrt{I}_m / \left(1 + 1.2 \sqrt{I_m} \right) \right], \quad (3\text{-}24)$$

$$B_{ca}^{\phi} = \beta_{ca}^{(0)} + \beta_{ca}^{(1)} \exp\left(-2 \sqrt{I_m} \right), \quad (3\text{-}25)$$

$$\left(\sum mz \right) = \sum_c m_c z_c = \sum_a m_a \left| z_a \right|, \quad (3\text{-}26)$$

where c is an index covering all cations, while a covers all anions [23]. The parameters $\beta_{ca}^{(0)}$ and $\beta_{ca}^{(1)}$ define the second virial coefficient, and C_{ca}^{ϕ} defines the third virial coefficient [24]. The values of those parameters were taken from Pitzer and Mayorga [24] ($\beta_{NaOH}^{(0)}$ = 0.0864, $\beta_{NaClO4}^{(0)}$ = 0.0554, $\beta_{NaOH}^{(1)}$ = 0.253, $\beta_{NaClO4}^{(1)}$ = 0.2755, C_{NaOH}^{ϕ}= 0.0044 and C_{NaClO4}^{ϕ}= −0.00118). The OH^- concentration is calculated from the amount of NaOH and H_2SeO_3 added to individual solutions. H_2SeO_3 is assumed to dissociate completely under high-pH conditions. During a cyclic voltammetry experiment, no O_2 gas bubble was found on the electrode. The value of pH_{obs} after the cyclic voltammetry experiment was the same as that before the cyclic voltammetry experiment. Therefore, it was considered that the cyclic voltammetry experiment made no changes in the OH^- concentration.

3.3.3 Results and discussion

Figure 3. 6 shows the cyclic voltammogram of the blank solution. A small peak at about −0.2 V vs. SHE and that at about 0.4 V vs. SHE are attributed to the formation of an oxide film on the electrode surface and to the corresponding reduction of the oxide film,

respectively. No voltammetric peaks associated with the redox reaction of NaOH or $NaClO_4$ are observed. Figure 3. 7 shows the cyclic voltammogram of a solution containing SeO_3^{2-} after repetitive potential cycling. The current is shifted in a positive direction by 10μA in the blank solution with m_{Na+} = 1.44 mol kg^{-1} (Figure 3. 6) and by 7μA in a solution with m_{Na+} = 0.96 mol kg^{-1} (Figure 3. 7). The positive shift of the current increases with increasing amount of the $NaClO_4$ reagent added to the individual solutions without further purification. This indicates the contribution of the impurities included in the $NaClO_4$ reagent to the current. In an electrochemical investigation using cyclic voltammetry to determine the plutonium (IV)/(III) standard redox potential, the cyclic voltammogram of a plutonium solution containing 1 mol dm^{-3} $NaClO_4$ supporting electrolyte also displayed a positive shift of the current [16].

As shown in Figure 3. 7, with increasing number of cycles, both the anodic and cathodic peaks appear clearly, consistent with electrochemical investigation of Se species, using cyclic voltammetry conducted with the working platinum electrode [10]. As described in section 3.2.3, this voltammetric behavior arises from a passivating layer covering the electrode surface. The cyclic voltammogram becomes steady by the 35th cycle. $E_{1/2}(T_0, I_m)$ is defined as the average of the five $E_{1/2}(T_0, I_m)$ values obtained from the 36th - 40th cyclic voltammograms. The uncertainty 1.96σ of these five $E_{1/2}(T_0, I_m)$ values, representing the 95% confidence level, is assigned to $E_{1/2}(T_0, I_m)$.

The peak shape of a cyclic voltammogram in Figure 3. 7 is broad. This feature corresponds to the diffusion of aqueous species [25]. To confirm this assignment, the anodic peak current of the 40th cyclic voltammogram after repetitive potential cycling is plotted as a function of $v^{1/2}$ in Figure 3. 8. The linear dependence of the anodic peak current on $v^{1/2}$ is also indicative of the diffusion-controlled process [19, 20]. The peak at about 0.3 V vs. SHE and

that at about −0.1 V vs. SHE are attributed to the oxidation of SeO_3^{2-} to SeO_4^{2-} and to the corresponding reduction of SeO_4^{2-} to SeO_3^{2-}, respectively.

An extra increase in the anodic current occurs in the potential range 0.18 ± 0.08 V vs. SHE. This potential range are shifted by − (*RT*/*F*log*e*) V pH^{-1} to 0.87 ± 0.08 V vs. SHE (pH = 1), where the stripping peak was observed in the cyclic voltammogram of a solution containing 1×10^{-3} mol dm^{-3} of SeO_2 [26]. The stripping peak is associated with the removal of a previously deposited film of Se [27] and can be considered independent of the oxidation of SeO_3^{2-} to SeO_4^{2-}. The anodic current is the sum of the current associated with the removal of the Se film and that associated with the oxidation of SeO_3^{2-} to SeO_4^{2-}. The cathodic wave is associated only with the corresponding reduction of SeO_4^{2-} to SeO_3^{2-}. The similarity in the peak shape between the anodic wave and the cathodic wave indicates that the contribution of the removal of Se film to the anodic current is not significant. Without subtracting this contribution from the total anodic current, the anodic peak current vs. $v^{1/2}$ plot shows a linear dependence (Figure 3. 8), as mentioned earlier. Therefore, the peak potential and current of the anodic wave were determined without any correction.

In the reversible case, E_p(Ox) and E_p(Red) remain constant even if the scan rate changes [17, 28]. In the quasi-reversible case, E_p(Ox) and E_p(Red) change with the scan rate, but $E_{1/2}(T_0, I_m)$ remains constant [16, 17]. E_p(Ox), E_p(Red) and $E_{1/2}(T_0, I_m)$ of the 40th cyclic voltammogram after repetitive potential cycling, measured at different scan rates in a solution containing SeO_3^{2-}, are listed in Table 3.2. As confirmed by the data in Table 3.2, the difference between E_p(Ox) and E_p(Red) increases with v, but $E_{1/2}(T_0, I_m)$ is independent of the scan rate. This feature corresponds to the quasi-reversible reaction. Assuming that $E_{1/2}(T_0, I_m)$ is the potential when the concentration of SeO_3^{2-} is equal to that of SeO_4^{2-}, Equation (3-9) is used to determine $E_{SeO4\ 2-/SeO3\ 2-}(T, 0)$.

The $E_{1/2}(T_0, I_m)$ values measured in alkaline sodium perchlorate solutions as a function of m_{Na+} are listed in Table 3.3. A plot of the Y_2 values vs. m_{Na+} is shown in Figure 3. 9. The values of $E_{SeO4\ 2-/SeO3\ 2-}(T_0, 0)$ and $\Delta\varepsilon_2$ are obtained by using the extrapolation of weighted linear regression [21] through Y_2 determined at various m_{Na+}, which corresponds to the line shown in Figure 3. 9. The intercept and slope of this line corresponds to $E_{SeO4\ 2-/SeO3\ 2-}(T_0, 0)$ and $\Delta\varepsilon_2$, respectively, given by

$E_{SeO4\ 2-/SeO3\ 2-}(T_0, 0) = 0.8227 \pm 0.0032$ V vs. SHE,

$\Delta\varepsilon_2 = 0.59 \pm 0.12$ kg mol^{-1}.

Olin et al. [6] indicated that under the experimental conditions used in Sherrill and Izard [5] the fraction of Se(IV) existing as H_2SeO_3 would vary in the range between 75 and 90 %. The corrected value of the equilibrium constant of Equation (3-3) based on this indication is $K = 1.1 \pm 0.1$. By combining this corrected value with the following $\Delta_r G^0{}_m$:

$HSeO_4^- \rightleftharpoons H^+ + SeO_4^{2-}$,

$\Delta_r G^0{}_m = 9.989 \pm 0.571$ kJ mol^{-1} (see [6]), (3-27)

$H_2SeO_3 \rightleftharpoons H^+ + HSeO_3^-$,

$\Delta_r G^0{}_m = 15.069 \pm 0.799$ kJ mol^{-1} (see [6]), (3-28)

$HSeO_3^- \rightleftharpoons H^+ + SeO_3^{2-}$,

$\Delta_r G^0{}_m = 47.719 \pm 1.313$ kJ mol^{-1} (see [6]), (3-29)

$Br_2 + 2e^- \rightleftharpoons 2Br^-$,

$\Delta_r G^0{}_m = -212.60 \pm 1.06$ kJ mol^{-1} (see [6]), (3-30)

$E_{SeO4\ 2-/SeO3\ 2-}(T_0, 0) = 0.8272 \pm 0.0315$ V vs. SHE is obtained. $E_{SeO4\ 2-/SeO3\ 2-}(T_0, 0) = 0.8267 \pm 0.0129$ V vs. SHE is obtained by combining $E_{SeO4\ 2-/HSeO3\ -}(T_0, 0)$ obtained by Doi and Yui [10, 11] (see section 3.2.3) with $\Delta_r G^0{}_m$ of Equation (3-29). These two calculated values are found to cover the entire range of $E_{SeO4\ 2-/SeO3\ 2-}(T_0, 0)$ obtained by this investigation. The result of

this investigation will make a contribution to more reliable prediction of the Se speciation at 25 °C in oxidized groundwater.

The value of $\varepsilon_{T0}(SeO_4^{2-}, Na^+)$ was estimated to be −0.12 ± 0.06 kg mol^{-1} using analogy with $\varepsilon_{T0}(SO_4^{2-}, Na^+)$ when Olin et al. [6] reviewed and compiled the thermodynamic data of Se. Because $\varepsilon_{T0}(SeO_3^{2-}, Na^+)$ is not available in the literature, this is also estimated to be equal to $\varepsilon_{T0}(SO_3^{2-}, Na^+)$ = −0.08 ± 0.05 kg mol^{-1} [6], by analogy, in this discussion. These ion interaction coefficients yield

$\Delta\varepsilon_2$ = − 0.04 ± 0.08 kg mol^{-1},

which dose not overlap the result of this investigation. An analogy with S would be inapplicable to estimate the ion interaction coefficient for Se species. Further investigations are needed to obtain the ion interaction coefficient for Se species. Therefore, a further investigation of Se, using cyclic voltammetry, has been carried out in order to obtain not the stoichiometric sum of ion interaction coefficient, but the ion interaction coefficient for Se species [14]. See section 3.4.

3.3.4 Conclusions

An electrochemical investigation, using cyclic voltammetry, has been carried out to determine the standard redox potential of the following redox reaction:

$$SeO_4^{2-} + 2H^+ + 2e^- \rightleftharpoons SeO_3^{2-} + H_2O\ .$$

The Se(VI)/(IV) half-wave potentials were measured in alkaline sodium perchlorate solutions as a fuction of m_{Na+}. Extrapolation of the experimental data to m_{Na+} = 0 using SIT yields the following standard redox potential and ion interaction coefficients:

$$E_{SeO4\ 2-/SeO3\ 2-}(T_0, 0) = 0.8227 \pm 0.0032 \text{ V vs. SHE},$$

$$\varepsilon_{T0}(SeO_4^{2-}, Na^+) - \varepsilon_{T0}(SeO_3^{2-}, Na^+) = 0.59 \pm 0.12 \text{ kg mol}^{-1}.$$

This standard redox potential is in good agreement with both $E_{SeO4\ 2-/HSeO3\ -}(T_0, 0)$ determined in section 3.2 and the corrected value of the equilibrium constant of the following reaction [5]:

$$Br_2 + H_2SeO_3 + H_2O \rightleftharpoons 3H^+ + HSeO_4^- + 2Br^- .$$

3.4 Determination of the molar entropy of the Se(VI)/(IV) couple

3.4.1. Experimental

Doi [14] used the glass cell (BAS Co., Ltd., 001056) composed of a circuit with a platinum working electrode (BAS Co., Ltd., 002013 PTE) with an exposed area of 3.1 mm^2, a platinum counter-electrode (BAS Co., Ltd., 002233 VC-3) and an Ag/AgCl reference electrode with a saturated solution of KCl (BAS Co., Ltd., 002058 RE-1C). The working electrode was polished using a 0.05μm alumina paste before each cyclic voltammetry experiment.

A solution of Se at a concentration of 9.3×10^{-4} mol kg^{-1} was prepared by the addition of Se standard (1003 mg dm^{-3} Se in 0.10 mol dm^{-3} HNO_3, Kanto Chemical Co., Inc., 37808-1B) and sodium nitrate ($NaNO_3$, Wako Jyunyaku Kogyo Co., Ltd., 195-02545) into 0.1000 mol dm^{-3} HNO_3. All reagents were used without further purification. The molality of Na^+ was adjusted to 0.500, 1.00, 1.50 and 2.00 mol kg^{-1}. The tetravalent Se species was H_2SeO_3 because the value of $-\log a_{H+}$ was estimated to be 1.13 ± 0.26 as described in section 3.4.2. The blank solution was prepared by dissolving $NaNO_3$ into 0.1000 mol dm^{-3} HNO_3 ($-\log a_{H+}$ = 1.11, m_{Na+} = 2.00 mol kg^{-1}). Aliquots of solution were transferred to the glass cell. The temperature of the solution in the glass cell was maintained by the thermostat water bath (AS ONE Co., Ltd., Thermax TM-1). The temperatures for the measurements were selected to be 15, 25, 35 and 50 °C because the values of $A(T)$ are available for these temperatures [13]. Before and after the cyclic voltammetry experiment, pH values at each temperature controlled by the thermostat water bath were measured using the combination glass pH electrode (TOA Co., Ltd., ION METER IM-55G). Because the reference electrode was immersed in the solution in the glass cell, it is reasonable to assume that the temperature of the internal

solution of the reference electrode was same as that of the solution in the glass cell. The scan rate was 0.6 V s^{-1} except while investigating the dependence of the peak current and potential on the scan rate. The scan region was 0.250 ↔ 1.240 V vs. Ag/AgCl, which corresponds to 0.449 ↔ 1.439 V vs. SHE at 25 °C, described as a solid line in Figure 3. 1.

3.4.2. Data analysis

Because $\varepsilon_T(i, j)$ are zero for uncharged species [6], using Equation (3-10), the value of $\log\gamma_{H2SeO3}$ was calculated to be zero. Therefore, the following relationship between $E_{1/2}(T, I_m)$ and $E_{HSeO4\text{-}/H2SeO3}(T, 0)$ can be obtained from Equation (3-9):

$$E_{1/2}(T, I_m) + E_{Ref}(T, I_{Ref}) = E_{HSeO4\text{-}/H2SeO3}(T, 0) + J\,(\log\gamma_{HSeO4\text{-}} + 3\log a_{H+} - \log a_{H2O}). \quad (3\text{-}31)$$

Application of Nernst's equation to the Ag/AgCl couple yields $E_{Ref}(T, I_{Ref})$ given by

$$E_{Ref}(T, I_{Ref}) = E_{Ag/AgCl}(T, 0) - J\,(2\log a_{Cl\text{-}}). \quad (3\text{-}32)$$

The value of $2\log a_{Cl\text{-}}$ in Equation (3-32) was equal to the common logarithm of the equilibrium constant, $\log K_1(T, 0)$, of the following reaction occurring in an internal solution of the Ag/AgCl reference electrode:

$$KCl \rightleftharpoons K^+ + Cl^- . \quad (3\text{-}33)$$

Cation that should be considered was Na^+ in a solution of Se. Using SIT, $\log\gamma_{HSeO4\text{-}}$ is calculated by

$$\log\gamma_{HSeO4\text{-}} = -D(T, I_m) + \varepsilon_T(HSeO_4^-, Na^+)m_{Na+}. \quad (3\text{-}34)$$

By substituting Equation (3-34) for $\log\gamma_{HSeO4\text{-}}$ in Equation (3-31), the following equations are finally obtained:

$$Y_3 = \varepsilon_T(HSeO_4^-, Na^+)m_{Na+} + Y_{intercept}\ , \quad (3\text{-}35)$$

where

$$Y_3 = E_{1/2}(T, I_m)/J + D(T, I_m) - 3\log a_{H+} + \log a_{H2O} \,, \quad (3\text{-}36)$$

$$Y_{\text{intercept}} = \{ E_{HSeO4\text{-}/H2SeO3}(T, 0) - E_{Ag/AgCl}(T, 0)\}/J + \log K_1(T, 0). \quad (3\text{-}37)$$

The values of Y_3 are plotted vs. m_{Na+}. As one would predict from Equation (3-35), the extrapolation of Y_3 to $m_{Na+} = 0$ gives a straight line where the slope and intercept correspond to $\varepsilon_T(HSeO_4^-, Na^+)$ and $Y_{\text{intercept}}$, respectively.

Measurements of $E_{1/2}(T, I_m)$ were made four times at each m_{Na+}. Using Equation (3-36), Y_3 was calculated from an average of $E_{1/2}(T, I_m)$, $E_{1/2}^{\text{ave}}(T, I_m)$. The uncertainty 1.96σ of the four measurements, representing the 95% confidence level, was assigned to $E_{1/2}^{\text{ave}}(T, I_m)$.

Because high ionic strength solution was used, pH_{obs} was not used to calculate Y_3. The value of $-\log a_{H+}$ is calculated by

$$-\log a_{H+} = -\log \gamma_{H+} - \log[H^+]. \quad (3\text{-}38)$$

The H^+ concentration is calculated from the amount of HNO_3. During the cyclic voltammetry experiment, no oxygen gas bubble was found on the electrode surface. The value of pH_{obs} after the cyclic voltammetry experiment was the same as that before the cyclic voltammetry experiment. Therefore, it was considered that the cyclic voltammetry experiment made no changes in the H^+ concentration. The value of $\log \gamma_{H+}$ is calculated using SIT as follows:

$$\log \gamma_{H+} = -D(T, I_m) + \varepsilon_T(NO_3^-, H^+) m_{NO3-} \,. \quad (3\text{-}39)$$

The value of $\varepsilon_{T0}(NO_3^-, H^+)$ is 0.07 ± 0.01 kg mol^{-1} [13]. The following relationship was proposed on the basis of a few experimental values for $\Delta\varepsilon_T(i, j)$ [29]:

$$\Delta\varepsilon_T(i, j) = \Delta\varepsilon_{T0}(i, j)\, T_0 / T \,. \quad (3\text{-}40)$$

Using Equation (3-40) with $\varepsilon_T(i, j)$ and $\varepsilon_{T0}(i, j)$ in place of $\Delta\varepsilon_T(i, j)$ and $\Delta\varepsilon_{T0}(i, j)$, the correction for $\varepsilon_{T0}(NO_3^-, H^+)$ was calculated to be less than 0.006 kg mol^{-1} for the temperature range of 15−50 °C. Because this correction was smaller than the assigned uncertainty in $\varepsilon_{T0}(NO_3^-, H^+)$, $\varepsilon_T(NO_3^-, H^+)$ at 15, 35 and 50°C was equal to $\varepsilon_{T0}(NO_3^-, H^+)$ in this study.

The values of $\log a_{H2O}$ were calculated using Equations (3-16), (3-23), (3-24), (3-25) and (3-26).

The $E_{Ag/AgCl}(T, 0)$ values are calculated using the following equation, which is applicable for any temperature from 0 to 95 °C [30]:

$$E_{Ag/AgCl}(T, 0) = 0.23695 - 4.8564\times10^{-4}T - 3.4205\times10^{-6}T^2 - 5.869\times10^{-9}T^3. \quad (3\text{-}41)$$

The standard molar Gibbs energy of formation of K^+ and Cl^- [6] and that of KCl [31] were used to calculate $\log K_1(T_0, 0)$. Equation (3-42) can be used to calculate equilibrium constant for any temperature from 0 to 200 °C [32].

$$\log K(T,0) = \log K(T_0,0) + \frac{\Delta_r H_m^0(T_0)}{R\ln(10)}\left(\frac{1}{T_0} - \frac{1}{T}\right) + \frac{\Delta_r C_{p,m}^0}{R\ln(10)}\left[\frac{T_0}{T} - 1 + \ln\left(\frac{T}{T_0}\right)\right]. \quad (3\text{-}42)$$

Equation (3-42) was used to calculate $\log K_1(T, 0)$ at 15, 35 and 50 °C. The standard molar enthalpy of formation of KCl, K^+ and Cl^- [31] were used to calculate $\Delta_r H^0_m(T_0)$ of Equation (3-33). Following the simplification that the heat capacity for any temperature is equal to that at 25 °C for the temperature range between 0 and 150 °C [32], the standard molar heat capacity of KCl, K^+ and Cl^- [31] were used to calculate $\Delta_r C^0_{p,m}$ of Equation (3-33)

The Gibbs-Helmholtz equation [17] is represented by

$$\left(\frac{\partial \Delta_r G_m^0}{\partial T}\right)_{p,n_i} = -\Delta_r S_m^0. \quad (3\text{-}43)$$

On the other hand,

$$\Delta_r G^0_m = -nFE_{Ox/Red}(T, 0). \quad (3\text{-}44)$$

Equation (3-45) is obtained by substituting Equation (3-44) into Equation (3-43) [17]:

$$\left(\frac{\partial E_{Ox/Red}(T,0)}{\partial T}\right)_{p,n_i} = \frac{\Delta_r S_m^0}{nF}. \quad (3\text{-}45)$$

Equation (3-45) indicates that the determination of $E_{Ox/Red}(T, 0)$ as a function of temperature

allows us to determine $\Delta_r S^0{}_m$.

3.4.3. Results and discussion

Figure 3. 10 shows the cyclic voltammogram of the blank solution. A small peak at about 1.0 V vs. Ag/AgCl and that at about 0.5 V vs. Ag/AgCl are attributed to the formation of an oxide film on the electrode surface and to the corresponding reduction of the oxide film, respectively.

Figure 3. 11 shows the cyclic voltammogram of a solution containing H_2SeO_3 after repetitive potential cycling. Peaks were assigned as arising from Se species present in solution. This was because no voltammetric peaks associated with the oxidation-reduction reaction of $NaNO_3$ and HNO_3 were observed in a voltammogram of the blank solution. With increasing number of cycles, two peaks appear clearly, consistent with electrochemical investigations of Se species, using cyclic voltammetry conducted with the working platinum electrode [10, 12]. As described in section 3.2.3, this voltammetric behavior arises from a passivating layer covering the electrode surface. The cyclic voltammogram became steady by the 35th cycle in this study. The $E_{1/2}(T, I_m)$ value was obtained from the 40th cyclic voltammogram.

The anodic peak current of the 40th cyclic voltammogram after repetitive potential cycling is plotted as a function of $v^{1/2}$ in Figure 3. 12. The linear dependence of the anodic peak current on $v^{1/2}$ is indicative of the diffusion-controlled process [19, 20]. The peak at about 1.0 V vs. Ag/AgCl and that at about 0.4 V vs. Ag/AgCl are attributed to the oxidation of H_2SeO_3 to $HSeO_4^-$ and to the corresponding reduction of $HSeO_4^-$ to H_2SeO_3, respectively.

Compared with the cathodic wave, an extra increase in the anodic current occurs in the potential range 0.87 ± 0.08 V vs. Ag/AgCl, where the stripping peak was observed in the cyclic voltammogram of a solution containing 1×10^{-3} mol dm^{-3} of SeO_2 [26]. Similar

behavior was observed in the cyclic voltammogram of a solution containing Se species (Figure 3. 7). The stripping peak is associated with the removal of a previously deposited film of Se [27] and can be considered independent of the oxidation of H_2SeO_3 to $HSeO_4^-$. The anodic current is the sum of the current associated with the removal of the Se film and that associated with the oxidation of H_2SeO_3 to $HSeO_4^-$. The cathodic wave is associated only with the corresponding reduction of $HSeO_4^-$ to H_2SeO_3. The similarity in the peak shape between the anodic wave and the cathodic wave indicates that the contribution of the removal of the Se film to the anodic current is not significant. Without subtracting this contribution from the total anodic current, evidence of a diffusion-controlled process was obtained as described earlier. These voltammetric features were seen from the voltammogram of a solution containing SeO_3^{2-} (see section 3.3.3). Therefore, as was the case of the cyclic voltammogram of a solution containing SeO_3^{2-}, the peak potential and current of the anodic wave were determined without any correction.

E_p(Ox), E_p(Red) and $E_{1/2}(T, I_m)$ of the 40th cyclic voltammogram after repetitive potential cycling, measured at different scan rates are listed in Table 3.4. As confirmed by the data in Table 3.4, $E_{1/2}(T, I_m)$ is independent of the scan rate. This feature corresponds to the quasi-reversible reaction [16, 17]. Assuming that $E_{1/2}(T, I_m)$ is the potential when the concentration of H_2SeO_3 is equal to that of $HSeO_4^-$, Equation (3-9) was used to determine $E_{\mathrm{HSeO4\ -/H2SeO3}}(T, 0)$ at each temperature.

Table 3.5 shows a summary of the cyclic voltammetry experiments to measure the half-wave potentials for the $HSeO_4^-/H_2SeO_3$ couple in acidic sodium nitrate solutions as a function of $m_{\mathrm{Na+}}$. A plot of the Y_3 values vs. $m_{\mathrm{Na+}}$ is shown in Figure 3. 13. The values of $Y_{\mathrm{intercept}}$ and $\varepsilon_T(HSeO_4^-, Na^+)$ are obtained by using the extrapolations of weighted linear regression [21] through Y determined at various $m_{\mathrm{Na+}}$, which correspond to the lines in Figure

3. 13. Using Equation (3-37), $E_{\mathrm{HSeO4\ -/H2SeO3}}(T, 0)$ were calculated from $Y_{\mathrm{intercept}}$, $E_{\mathrm{Ag/AgCl}}(T, 0)$ and log $K_1(T, 0)$. The values of $Y_{\mathrm{intercept}}$, $\varepsilon_T(\mathrm{HSeO_4^-}, \mathrm{Na^+})$, $E_{\mathrm{Ag/AgCl}}(T, 0)$, log $K_1(T, 0)$ and $E_{\mathrm{HSeO4\ -/H2SeO3}}(T, 0)$ are listed in Table 3.6. A plot of the $E_{\mathrm{HSeO4\ -/H2SeO3}}(T, 0)$ values vs. temperature is shown in Figure 3. 14, where the solid line represents a weighted linear regression [21] of $E_{\mathrm{HSeO4\ -/H2SeO3}}(T, 0)$. The slope of this line corresponds to $\Delta_r S^0{}_m /2F$ given by

$\Delta_r S^0{}_m /2F = -0.3 \pm 0.1$ mV °C^{-1}.

The OECD/NEA-selected values for the standard molar enthalpy of the formation of $\mathrm{HSeO_4^-}$, $\mathrm{H_2SeO_3}$ and $\mathrm{H_2O}$ are −582.700 ± 4.700 kJ mol^{-1}, −505.320 ± 0.650 kJ mol^{-1} and −285.830 ± 0.040 kJ mol^{-1}, respectively [6]. From these values, $\Delta_r H^0{}_m(T_0)$ of Equation (3-7) was calculated to be −208.450 ± 4.745 kJ mol^{-1}. This calculated value was compared with the $\Delta_r H^0{}_m(T_0)$ value calculated from our experimental results. The following relationship permits calculation of $\Delta_r H^0{}_m$:

$$\Delta_r G^0{}_m = \Delta_r H^0{}_m - T\,\Delta_r S^0{}_m \,. \qquad (3\text{-}46)$$

Using Equation (3-44), $\Delta_r G^0{}_m(T_0)$ of Equation (3-7) was calculated to be −196.85 ± 0.69 kJ mol^{-1} from $E_{\mathrm{HSeO4\ -/H2SeO3}}(T_0, 0)$ listed in Table 3.6. Using Equation (3-46), from $\Delta_r G^0{}_m(T_0)$ and $\Delta_r S^0{}_m$ obtained by this study using cyclic voltammetry, $\Delta_r H^0{}_m(T_0)$ of Equation (3-7) was calculated to be −212 ± 6 kJ mol^{-1}, which agrees with the $\Delta_r H^0{}_m(T_0)$ value calculated from the OECD/NEA-selected values within the uncertainty limits. The result of this study will make a contribution to more reliable prediction of the Se speciation at a temperature over 25 °C in oxidized groundwater.

The value of $\varepsilon_{T0}(\mathrm{HSeO_4^-}, \mathrm{Na^+})$ was determined to be 0.29 ± 0.03 kg mol^{-1}. Available literature values for $\varepsilon_{T0}(\mathrm{HSO_4^-}, \mathrm{Na^+})$ are −0.01 ± 0.02 kg mol^{-1} [6] and 0.11 ± 0.05 kg mol^{-1} [33]. The difference was found between $\varepsilon_{T0}(\mathrm{HSeO_4^-}, \mathrm{Na^+})$ and $\varepsilon_{T0}(\mathrm{HSO_4^-}, \mathrm{Na^+})$. The ion

interaction coefficient is dependent on the size and charge of the ion [13]. The relationship between the size of monovalent anions and the ion interaction coefficient for Na^+ was surveyed. We compare the ionic radius of F^-, Cl^-, Br^- and I^-, which increase in that order [34]. This order is the same as found for the magnitude of the ion interaction coefficient for Na^+, i.e., $\varepsilon_{T0}(F^-, Na^+) < \varepsilon_{T0}(Cl^-, Na^+) < \varepsilon_{T0}(Br^-, Na^+) < \varepsilon_{T0}(I^-, Na^+)$ [13]. Among these monovalent anions, the larger the size, the larger the magnitude of the ion interaction coefficient for Na^+ is. The ionic radius of Se^{6+} is longer than that of S^{6+} [34]. From the fact that the interatomic distances of H_2Se, SeO_4^{2-} and SeO_2 are longer than those of H_2S, SO_4^{2-} and SO_2, respectively [35], the interatomic distances of $HSeO_4^-$ are considered to be longer than those of HSO_4^-. Therefore, the size of $HSeO_4^-$ is likely to be larger than that of HSO_4^-, which is consistent with the relationship of $\varepsilon_{T0}(HSeO_4^-, Na^+) > \varepsilon_{T0}(HSO_4^-, Na^+)$.

A plot of the $\varepsilon_T(HSeO_4^-, Na^+)$ values vs. temperature is shown in Figure 3. 15. The value of $\partial\varepsilon/\partial T$ was obtained by using the extrapolation of weighted linear regression [21] through $\varepsilon_T(HSeO_4^-, Na^+)$ obtained at 15, 25, 35 and 50 °C, which corresponds to the line in Figure 3. 15. The slope of this line corresponds to $\partial\varepsilon/\partial T$ given by

$\partial\varepsilon/\partial T = -0.002 \pm 0.002$ kg mol^{-1} °C^{-1}.

The temperature dependence of the ion interaction coefficient was discussed by Lewis and Randall [36], Millero [37], Helgeson et al. [38], Oelkers and Helgeson [39] and Grenthe and Plyasunov [40]. All these studies reported that $\partial\varepsilon/\partial T$ are usually ≤ 0.005 kg mol^{-1} °C^{-1} for temperatures below 200 °C, which is consistent with our result. The small temperature dependence of $\varepsilon_T(HSeO_4^-, Na^+)$ suggests that the change in the interatomic distance of $HSeO_4^-$ is small for the temperature range of 15−50 °C, which is consistent with the fact that the change in the interatomic distance associated with a temperature change of 50° is less than 0.01Å [41].

3.4.4. Conclusions

An electrochemical investigation of selenium species, using cyclic voltammetry, has been carried out for the purpose of determining the molar entropy of the Se(VI)/(IV) couple. To obtain the value for $\varepsilon_T(HSeO_4^-, Na^+)$, the following reaction involving $HSeO_4^-$ as the oxidant and the H_2SeO_3 uncharged species as the reductant was used:

$$HSeO_4^- + 3H^+ + 2e^- \rightleftharpoons H_2SeO_3 + H_2O\ .$$

The Se(VI)/(IV) half-wave potentials were measured in acidic sodium nitrate solutions as functions of m_{Na+} ranging from 0.500 to 2.00 mol kg^{-1} and temperature ranging from 15 to 50 °C. SIT was used to calculate $E_{HSeO4\ -/H2SeO3}(T, 0)$ and $\varepsilon_T(HSeO_4^-, Na^+)$. The following molar entropy was derived from the temperature dependence of $E_{HSeO4\ -/H2SeO3}(T, 0)$:

$$\Delta_r S^0_m /2F = -0.3 \pm 0.1 \text{ mV °C}^{-1}.$$

The value of $\varepsilon_T(HSeO_4^-, Na^+)$ at 25 °C was determined to be 0.29 ± 0.03 kg mol^{-1}. The following $\partial\varepsilon/\partial T$ was derived from the temperature dependence of $\varepsilon_T(HSeO_4^-, Na^+)$:

$$\partial\varepsilon/\partial T = -0.002 \pm 0.002 \text{ kg mol}^{-1} \text{ °C}^{-1}.$$

References in Chapter 3.

1. Chunming S, Donald LS. [Selenate and selenite sorption on iron oxides an infrared and electrophoretic study]. Soil. Sci. Soc. Am. J. 2000; 64 No. 1:101-111.
2. Cui D, Puranen A, Devoy J, Scheidegger A, Leupin OX, Wersin P, Gens R, Spahiu K. [Reductive immobilization of ^{79}Se by iron canister under simulated repository environment]. J. Radioanal. Nucl. Chem. 2009; 282:349-354.
3. Japan Nuclear Cycle Development Institute (JNC). H12: project to establish the scientific and technical basis for HLW disposal in Japan - second progress report on research and development for the geological disposal of HLW in Japan. Japan: Japan Nuclear Cycle Development Institute (JNC); 2000.
4. Runnells DD, Lindberg RD, Kempton JH. [Irreversibility of Se(VI)/Se(IV) redox couple in synthetic basaltic ground water at 25°C and 75°C]. Mater. Res. Soc. Symp. Proc. 1987; 84:723-733.
5. Sherrill MS, Izard EF. [The reduction potential of selenous acid and the free energy of aqueous selenic acid]. J. Am. Chem. Soc. 1928; 50:1665-1675.
6. Olin Å, Noläng B, Öhman LO, Osadchii EG, Rosén E. Chemical Thermodynamics of Selenium. Amsterdam: ELSEVIER; 2005.
7. Milne J, Lahaie P. [Chloroselenate(IV) equilibria in aqueous hydrobromic acid]. Inorg. Chem. 1979; 18:3180-3183.
8. Milne J. [Haloselenate(IV) formation and selenous acid dissociation equilibria in hydrochloric and hydrofluoric acids]. Can. J. Chem. 1987; 65:316-321.
9. Milne J, Lahaie P. [Bromoselenate(IV) equilibria in aqueous hydrobromic acid]. Inorg. Chem. 1985; 24:840-844.

10. Doi R, Yui M. [Experimental study by cyclic voltammetry of standard potential of Se(IV)/Se(VI) redox system]. Journal of Nuclear Fuel Cycle and Environment. 2009; 16 No. 1:35-42 [in Japanese].
11. Doi R. [Errata to "Experimental study by cyclic voltammetry of standard potential of Se(IV)/Se(VI) redox system"]. Journal of Nuclear Fuel Cycle and Environment. 2012; 19 No. 2:65-66 [in Japanese].
12. Doi R. [Determination of the selenium (VI)/(IV) standard redox potential by cyclic voltammetry]. J. Nucl. Sci. Technol. 2014; 51 No.1:56-63. (published online: 21 October 2013)
13. Grenthe I, Mompean F, Spahiu K, Wanner H. TDB-2 guidelines for the extrapolation to zero ionic strength. Issy-les-Moulineaux (France): OECD Nuclear Energy Agency; 2013. Available from: http://www.oecd-nea.org/dbtdb/guidelines/tdb2.pdf
14. Doi R. [Molar entropy of the selenium (VI)/(IV) couple obtained by cyclic voltammetry]. J. Nucl. Sci. Technol. (published online: 9 January 2014)
15. Philippini V, Aupiais J, Vercounter T, Moulin C (2009) Formation of $CaSO_4$(aq) and $CaSeO_4$(aq) studied as a function of ionic strength and temperature by CE. ELECTROPHORESIS 20:3582-3590
16. Riglet CH, Robouch P, Vitorge P. [Standard potentials of the (MO_2^{2+}/MO_2^{+}) and (M^{4+}/M^{3+}) redox systems for Neptunium and Plutonium]. Radiochim. Acta. 1989;46:85-94.
17. Capdevila H, Vitorge P. [Temperature and ionic strength influence on U(VI/V) and U(IV/III) redox potentials in aqueous acidic and carbonate solutions]. Journal of Radioanalytical and Nuclear Chemistry. 1990; 143 No. 2:403-414.
18. Tomas V, Pierre V, Badia A, Eric G, Solange H, Christophe M. [Stabilities of the

aqueous complexes $Cm(CO_3)_3^{3-}$ and $Am(CO_3)_3^{3-}$ in the temperature range 10-70°C]. Inorg. Chem. 2005;44:5833-5843

19. Kim SY, Asakura T, Morita Y. [Electrochemical and spectroscopic studies of Pu(IV) and Pu(III) in nitric acid solutions]. J. Radioanal. Nucl. Chem. 2013; 295:937-942.
20. Fujishima A, Aizawa M, Inoue T. Electrochemical measurements. Tokyo: Gihodo Syuppan Co.; 1984.
21. Wanner H, Östhols E. TDB-3 guidelines for the assignment of uncertainties. Issy-les-Moulineaux (France): OECD Nuclear Energy Agency; 2000. Available from:-http://www.oecd-nea.org/dbtdb/guidelines/tdb3new.pdf
22. Stumm W, Morgan JJ. Aquatic Chemistry, 3rd edition. New York: John Wiley & Sons; 1996.
23. Pitzer KS, Kim JJ. [Thermodynamics of electrolytes. IV. Activity and osmotic coefficients for mixed electrolytes]. J. Am. Chem. Soc. 1974; 96:5701-5707.
24. Pitzer KS, Mayorga G. [Thermodynamics of electrolytes. II. Activity and osmotic coefficients for strong electrolytes with one or both ions univalent]. J. Phys. Chem. 1976; 77:2300-2308.
25. Grégoire H, Victor K, Damien WMA. [Electrochemical behavior of haemoglobin at the liquid/liquid interface]. Electrochim. Acta. 2008; 53:7204-7209.
26. Murat A, Umit D, Curtis S. [Electrochemical formation of Se atomic layers on Au(1 1 1) surface: the role of adsorbed selenate and selenite]. J. Electroanal. Chem. 2004; 561:21-27.
27. Andrews RW, Johnson DC. [Voltammetric deposition and stripping of selenium(IV) at a rotating gold-disk electrode in 0.1M perchloric acid]. Anal. Chem. 1975; 47:294-299.
28. Watanebe T, Nakabayashi S. Electron transfer chemistry - Introduction to

electrochemistry. Tokyo: Asakura Syoten Co.; 1996. 9. Bunshi-ionnonagare; p.168 [in Japanese].

29. Tomas V, Pierre V, Badia A, Eric G, Solange H, Christophe M. [Stabilities of the aqueous complexes $Cm(CO_3)_3^{3-}$ and $Am(CO_3)_3^{3-}$ in the temperature range 10-70°C]. Inorg. Chem. 2005; 44:5833-5843.
30. Bard J, Parsons R, Jordan J. Standard potentials in aqueous solution. New York (NY): Marcel Dekker, Inc;1986.
31. Wagman DD, Evans WH, Parker VB, Schumm RH, Halow I, Bailey SM, Churney KL, Nuttall RL. The NBS tables of chemical thermodynamic properties: selected values for inorganic and C_1 and C_2 organic substances in SI units. New York (NY): American Chemical Society and American Institute of Physics; 1982.
32. Puigdomènech I, Rard JA, Plyasunov AV, Grenthe I. TDB-4 temperature corrections to thermodynamic data and enthalpy calculations Issy-les-Moulineaux (France): OECD Nuclear Energy Agency; 1999. Available from: http://www.oecd-nea.org/dbtdb/guidelines/tdb4new.pdf
33. Tomas V, Badia A, Christophe M, Eric G, Pierre V. [Sulfate complexation of trivalent lanthanides probed by nanoelectrospray mass spectrometry and time-resolved laser induced luminescence]. Inorg. Chem. 2005; 44:7570-7581.
34. Shannon RD. [Revised effective ionic radii and systematic studies of interatomic distances in halides and chalcogenides]. Acta Crystallogr Sect 1976; A 32:751-767.
35. The Chemical Society of Japan. Chemical handbook. Tokyo (Japan): Maruzen Publishing Co. Ltd.; 1993.
36. Lewis GN, Randall M. Thermodynamics. 2nd ed. Revised by Pitzer KS. and Brewer L. New York (NY): McGraw-Hill; 1961.

37. Millero FJ. Effects of pressure and temperature on activity coefficients. In: Pytkowicz RM, editor. Activity coefficients in electrolyte solutions. Boca Raton (FL): CRC Press; 1979.
38. Helgeson HC, Kirkham DH, Flowers GC. [Theoretical prediction of the thermodynamic behavior of aqueous electrolytes at high pressures and temperatures: IV. Calculation of activity coefficients, osmotic coefficients, and apparent molal and standard and relative partial molal properties to 600°C and 5 kb]. Am. J. Sci. 1981; 281:1249-1516.
39. Oelkers EH, Helgeson HC. [Triple-ion anions and polynuclear complexing in supercritical electrolyte solutions]. Geochim. Cosmochim. Acta. 1990; 54:727-738.
40. Grenthe I, Plyasunov A. [On the use of semiempirical electrolyte theories for the modeling of solution chemical data]. Pure. Appl. Chem. 1997; 69:951-958.
41. Xiangliang, Siagian S, Basar K, Sakuma T, Takahashi H, Igawa N, Ishii Y. [Inter-atomic distance and temperature dependence of correlation effects among thermal displacements]. Solid State Ionics 2009; 180:480-482.

Tables and Figures in Chapter 3.

Table 3.1. Summary of cyclic voltammetry experiments to measure the half-wave potentials for the $SeO_4^{2-}/HSeO_3^-$ couple in acidic sodium perchlorate solutions as a function of m_{Na+}.

m_{Na+} (mol kg^{-1})	pH_{obs} [a]	T (°C)	D(20°C, I_m) [b]	D(25°C, I_m) [c]	$E_{1/2}(T, I_m)$ (V vs. SHE)	Y_1(20°C) [d]	Y_1(25°C) [e]
2.00	3.0	22.3	0.229	0.231	0.8395±0.0005	38.30±0.02	38.30±0.02
2.00	2.9	21.8	0.229	0.231	0.8245±0.0010	37.53±0.04	37.54±0.04
1.50	3.1	20.7	0.218	0.220	0.8260±0.0010	38.27±0.05	38.27±0.05
1.00	3.0	25.0	0.202	0.204	0.8340±0.0005	37.79±0.02	37.79±0.02
1.00	3.0	25.0	0.202	0.204	0.8220±0.0010	37.38±0.05	37.39±0.05
0.500	3.0	25.0	0.173	0.175	0.8080±0.0007	36.83±0.02	36.83±0.02
0.500	2.8	25.0	0.173	0.175	0.8105±0.0010	36.31±0.04	36.32±0.04

Note: [a] pH_{obs} was the result of the pH measurement performed by the pH meter before each cyclic voltammetry experiment, [b, c] Using Equation (3-11), D(20°C, I_m) and D(25°C, I_m) was calculated from a combination of A(20°C) and B(20°C) and that of A(25°C) and B(25°C), respectively, [d] $Y_1(20°C) = \{E_{1/2}(T, I_m) + E_{Ref}(T_0, I_{Ref})\}/J + 3D(20°C, I_m) + 3pH_{obs} + \log a_{H2O}$, [e] $Y_1(25°C) = \{E_{1/2}(T, I_m) + E_{Ref}(T_0, I_{Ref})\}/J + 3D(25°C, I_m) + 3pH_{obs} + \log a_{H2O}$, where $E_{Ref}(T_0, I_{Ref})$ = 0.241 V vs. SHE in case of the saturated calomel reference electrode with a saturated solution of KCl, $J = RT/2F \log e$.

Table 3.2. E_p(Ox), E_p(Red) and $E_{1/2}(T_0, I_m)$ of the 40th cyclic voltammogram after repetitive potential cycling, measured at different scan rates in a solution containing SeO_3^{2-}.

v (V s^{-1})	E_p(Ox) (V vs. Hg/HgO)	E_p(Red) (V vs. Hg/HgO)	$E_{1/2}(T_0, I_m)$ (V vs. Hg/HgO)
0.12	0.2157	−0.2189	-0.0016
0.11	0.2092	−0.2124	-0.0016
0.09	0.2009	−0.2043	-0.0017
0.08	0.2001	−0.2035	-0.0017
0.07	0.1993	−0.2027	-0.0017
0.06	0.1928	−0.1961	-0.0017

Table 3.3. Summary of cyclic voltammetry experiments to measure the half-wave potentials for the SeO_4^{2-}/SeO_3^{2-} couple in alkaline sodium perchlorate solutions as a function of m_{Na+}.

m_{Na+} (mol kg^{-1})	T (°C)	[OH$^-$] (mol dm^{-3})	I_m (mol kg^{-1})	$-\log a_{H+}$	$E_{1/2}(T_0, I_m)$ (V vs. SHE)	Y_2 [a]
0.10	24.6	0.066±0.002	0.11	12.71±0.01	0.067±0.004	27.67±0.13
0.10	25.0	0.066±0.002	0.11	12.71±0.01	0.079±0.006	28.08±0.20
0.48	25.3	0.065±0.002	0.49	12.66±0.01	0.081±0.005	28.07±0.17
0.48	24.5	0.065±0.002	0.49	12.66±0.01	0.087±0.004	28.27±0.14
0.96	25.3	0.063±0.002	0.97	12.65±0.02	0.094±0.005	28.44±0.18
0.96	25.1	0.073±0.002	0.97	12.71±0.02	0.087±0.006	28.35±0.20
1.45	24.9	0.071±0.002	1.45	12.71±0.02	0.095±0.004	28.61±0.16
1.45	24.9	0.071±0.002	1.45	12.71±0.02	0.096±0.006	28.63±0.21

Note: [a] $Y_2 = \{E_{1/2}(T_0, I_m) + E_{Ref}(T_0, I_{Ref})\}/J - 2\log a_{H+} + \log a_{H2O}$, where $E_{Ref}(T_0, I_{Ref}) = 0.105$ V vs. SHE (calculated using SIT) in case of the Hg/HgO reference electrode in a solution of 1 mol dm^{-3} NaOH, $J = RT/2F \log e$.

Table 3.4. E_p(Ox), E_p(Red) and $E_{1/2}(T, I_m)$ of the 40th cyclic voltammogram after repetitive potential cycling, measured at different scan rates in a solution containing H_2SeO_3 ($-\log a_{H+}$ = 1.15, m_{Na+} = 1.00 mol kg^{-1}, 24.5 °C).

v (V s^{-1})	E_p(Ox) (V vs. Ag/AgCl)	E_p(Red) (V vs. Ag/AgCl)	$E_{1/2}(T, I_m)$ (V vs. Ag/AgCl)
0.80	1.0535	0.3992	0.7264
0.60	1.0515	0.4009	0.7262
0.50	1.0408	0.4118	0.7263
0.40	1.0372	0.4153	0.7263
0.30	1.0319	0.4207	0.7263
0.20	1.0247	0.4279	0.7263
0.10	1.0247	0.4279	0.7263
0.08	1.0247	0.4279	0.7263

Table 3.5. Summary of the cyclic voltammetry experiments to measure the half-wave potentials for the $HSeO_4^-/H_2SeO_3$ couple in acidic sodium nitrate solutions as a function of m_{Na+}.

T (°C)	m_{Na+} (mol kg^{-1})	$D(T, I_m)$ [a]	$-\log a_{H+}$	$\log a_{H2O}$	$E_{1/2}^{ave}(T, I_m)$ [b] (V vs. Ag/AgCl)	Y_3 [c]
15.3±0.6	0.500	0.18	1.14±0.00	−0.0083	0.7137±0.0025	28.65±0.09
	1.00	0.20	1.14±0.01	−0.0148	0.7200±0.0035	28.75±0.13
	1.50	0.22	1.13±0.01	−0.0212	0.7274±0.0010	28.95±0.04
	2.00	0.23	1.11±0.01	−0.0275	0.7332±0.0009	29.15±0.05
25.2±1.1	0.500	0.18	1.15±0.00	−0.0083	0.7137±0.0000	27.90±0.01
	1.00	0.21	1.15±0.01	−0.0148	0.7269±0.0022	28.23±0.08
	1.50	0.22	1.14±0.01	−0.0212	0.7290±0.0001	28.21±0.04
	2.00	0.23	1.12±0.01	−0.0275	0.7332±0.0017	28.28±0.07
35.0±1.4	0.500	0.19	1.16±0.00	−0.0083	0.7222±0.0009	27.22±0.07
	1.00	0.21	1.16±0.01	−0.0148	0.7276±0.0010	27.48±0.04
	1.50	0.23	1.14±0.01	−0.0212	0.7324±0.0009	27.59±0.06
	2.00	0.24	1.13±0.01	−0.0275	0.7371±0.0020	27.73±0.08
50.3±0.5	0.500	0.19	1.17±0.00	−0.0083	0.7283±0.0009	26.40±0.03
	1.00	0.22	1.16±0.01	−0.0148	0.7326±0.0000	26.51±0.03
	1.50	0.23	1.15±0.01	−0.0212	0.7362±0.0000	26.60±0.03
	2.00	0.24	1.13±0.01	−0.0275	0.7436±0.0009	26.80±0.05

Note: [a] $D(T, I_m)$ is Debye-Hückel term [13], [b] $E_{1/2}^{ave}(T, I_m)$ is an average of $E_{1/2}(T, I_m)$ in four measurements at each m_{Na+}, [c] $Y = E_{1/2}^{ave}(T, I_m)/J + D(T, I_m) - 3\log a_{H+} + \log a_{H2O}$, where $J = RT/2F\log e$.

Table 3.6. Values of $Y_{\text{intercept}}$, $\varepsilon_T(HSeO_4^-, Na^+)$, $E_{Ag/AgCl}(T, 0)$, $\log K_1(T, 0)$ and $E_{HSeO4\text{-}/H2SeO3}(T, 0)$. The intercept and slope of each line in Figure 3. 13 correspond to $Y_{\text{intercept}}$ and $\varepsilon_T(HSeO_4^-, Na^+)$, respectively, at each temperature.

T (°C)	$Y_{\text{intercept}}$ [a]	$\varepsilon_T(HSeO_4^-, Na^+)$ (kg mol^{-1})	$E_{Ag/AgCl}(T, 0)$ (V vs. SHE)	$\log K_1(T, 0)$ [b]	$E_{HSeO4\text{-}/H2SeO3}(T, 0)$ (V vs. SHE)
15.3±0.6	28.44±0.10	0.35±0.06	0.2287±0.0003	0.697±0.041	1.0226±0.0037
25.2±1.1	27.76±0.03	0.29±0.03	0.2225±0.0006	0.805±0.055	1.0203±0.0035
35.0±1.4	27.12±0.08	0.32±0.06	0.2155±0.0008	0.897±0.065	1.0171±0.0049
50.3±0.5	26.26±0.04	0.25±0.03	0.2031±0.0003	1.012±0.035	1.0133±0.0022

Note: [a] $Y_{\text{intercept}} = \{E_{HSeO4\text{-}/H2SeO3}(T, 0) - E_{Ag/AgCl}(T, 0)\}/J + \log K_1(T, 0)$, where $J = RT/2F\log e$, [b] $K_1(T, 0)$ is the equilibrium constant of the reaction ($KCl \rightleftharpoons K^+ + Cl^-$) occurring in an internal solution of the Ag/AgCl reference electrode.

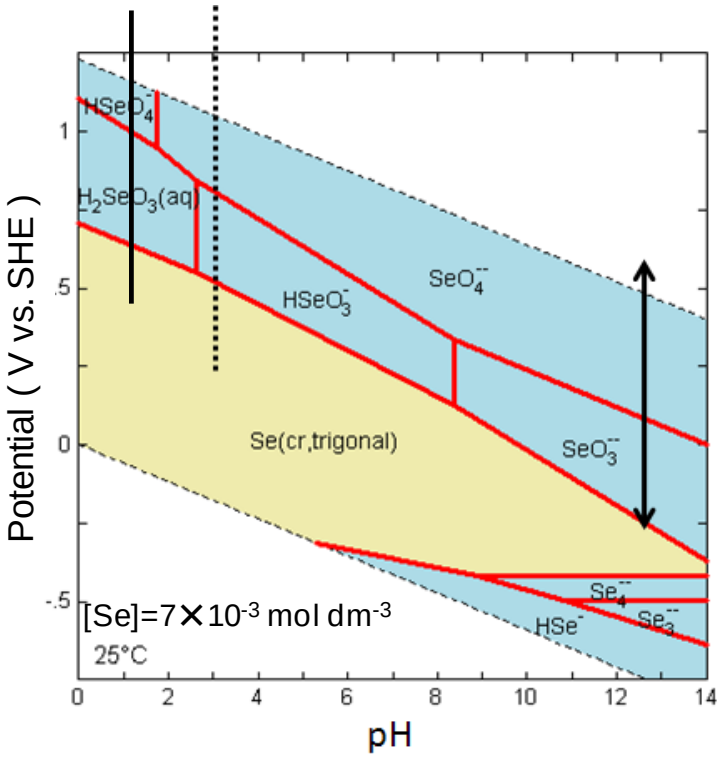

Figure 3. 1. Potential-pH diagram for Se system based on the thermodynamic data compiled by Olin et al. [6]. The total concentration of Se is 7×10^{-3} mol dm^{-3}. The vertical dotted line, the line with arrow points and the solid line indicate the scan region in Doi and Yui [10] (0.241 ↔ 1.441 V vs. SHE and $pH_{obs} = 3.0 \pm 0.2$), that in Doi [12] (−0.293 ↔ 0.606 V vs. SHE and $-\log a_{H+} = 12.68 \pm 0.05$) and that in Doi [14] (0.449 ↔ 1.439 V vs. SHE and $-\log a_{H+} = 1.13 \pm 0.26$), respectively.

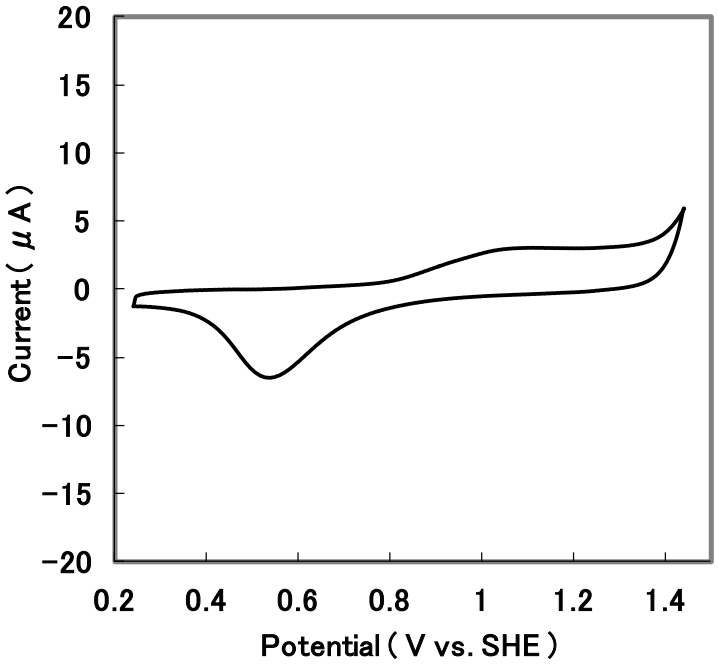

Figure 3. 2. Cyclic voltammogram of the blank solution ($[HNO_3] = 8 \times 10^{-4}$ mol dm^{-3}).

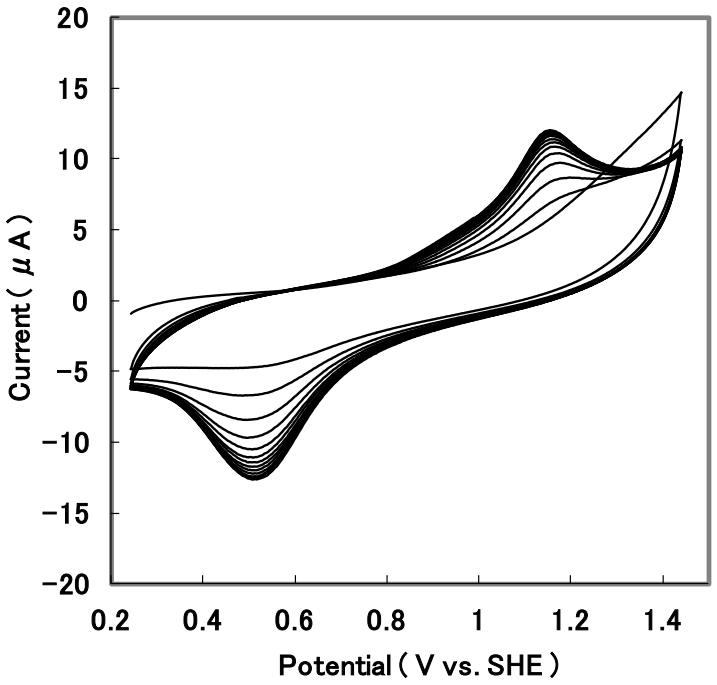

Figure 3. 3. Cyclic voltammogram of a solution containing $HSeO_3^-$ after repetitive potential cycling ([Se] = 1.00×10^{-4} mol dm^{-3}, pH_{obs} = 3.0, I_m = 1.00 mol kg^{-1}, 25.3 °C).

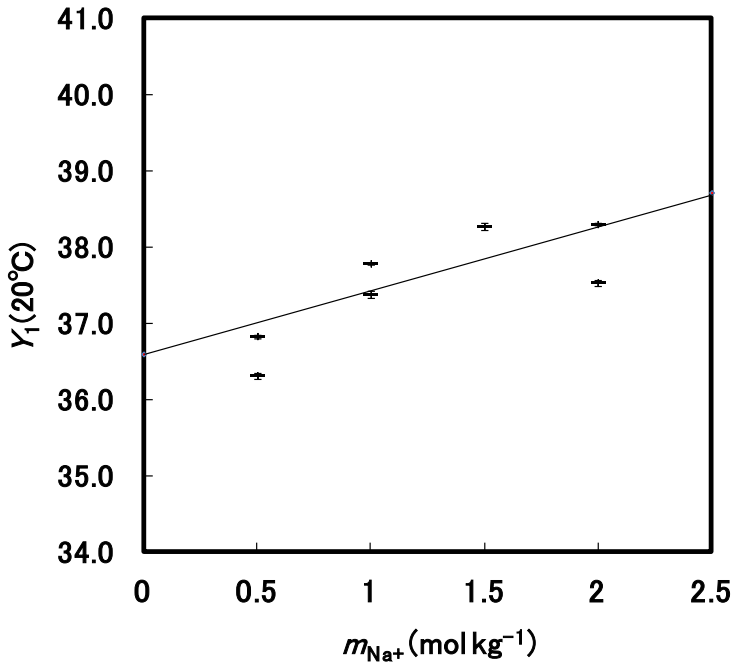

Figure 3. 4. Determination of the standard redox potential for the $SeO_4^{2-}/HSeO_3^-$ couple using the specific ion interaction theory. Experimental data as a function of m_{Na+} is shown as the solid bars. The solid line is the weighted linear regression fit [21] of data. The slope and intercept of this line correspond to $\Delta\varepsilon_1$ and $E_{SeO4\ 2-/HSeO3\ -}(T_0, 0)/J$, respectively. Y_1 (20°C) = $\{E_{1/2}(T, I_m) + E_{Ref}(T_0, I_{Ref})\}/J + 3D(20°C, I_m) + 3pH_{obs} + \log a_{H2O}$, where $J = RT/2F \log e$.

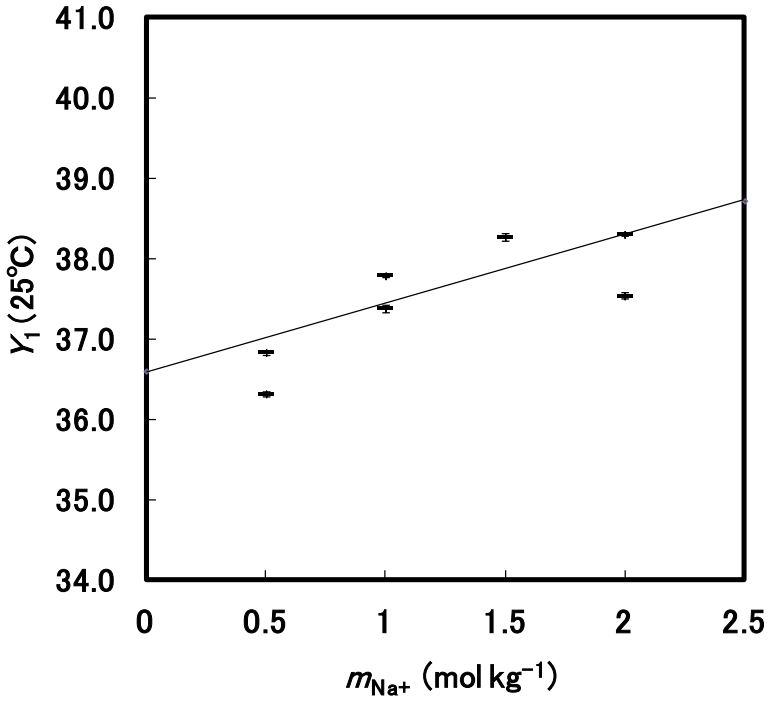

Figure 3. 5. Determination of the standard redox potential for the $SeO_4^{2-}/HSeO_3^-$ couple using the specific ion interaction theory. Experimental data as a function of m_{Na+} is shown as the solid bars. The solid line is the weighted linear regression fit [21] of data. The slope and intercept of this line correspond to $\Delta\varepsilon_1$ and $E_{SeO4\ 2-/HSeO3\ -}(T_0, 0)/J$, respectively. Y_1 (25°C) = $\{E_{1/2}(T, I_m) + E_{Ref}(T_0, I_{Ref})\}/J + 3D(25°C, I_m) + 3pH_{obs} + \log a_{H2O}$, where $J = RT/2F \log e$.

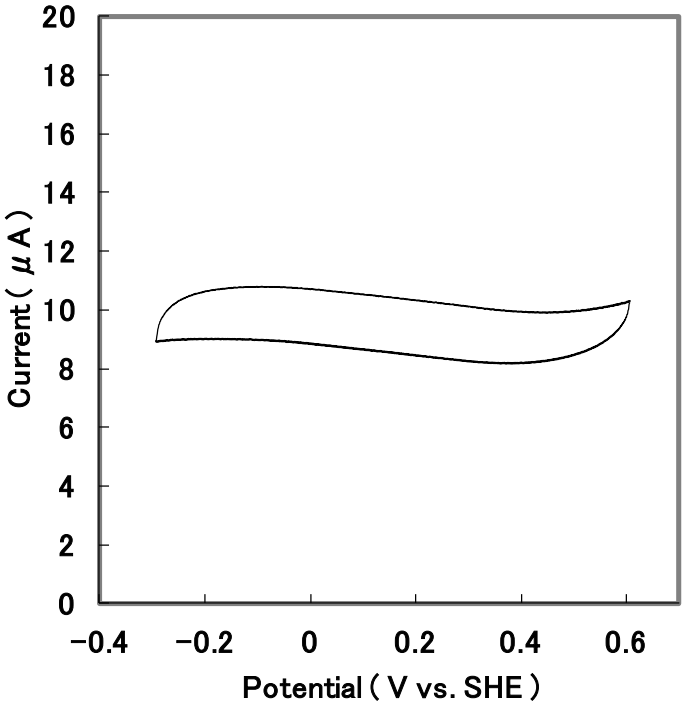

Figure 3. 6. Cyclic voltammogram of the blank solution ($-\log a_{H^+}$ = 12.90 ± 0.02, m_{Na^+} = 1.44 mol kg^{-1}, 25.0 °C).

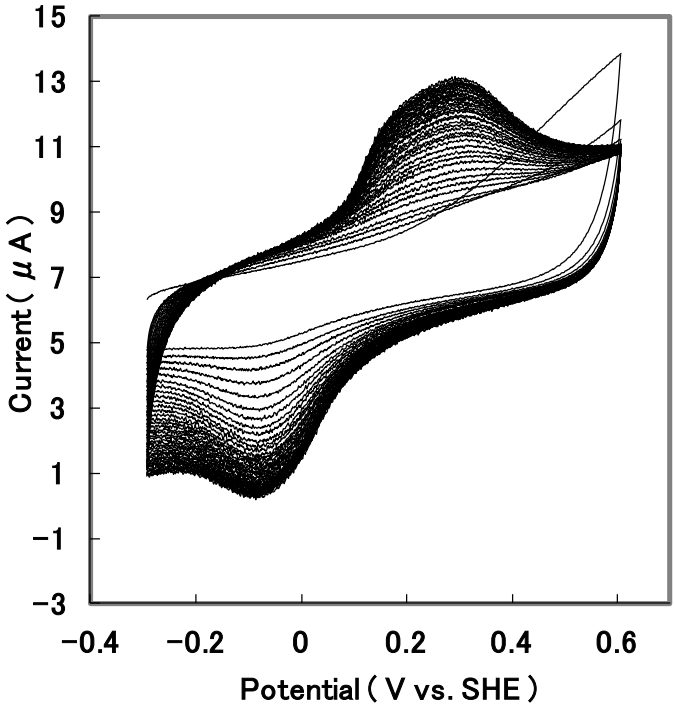

Figure 3. 7. Cyclic voltammogram of a solution containing SeO_3^{2-} after repetitive potential cycling ($-\log a_{H+}$ = 12.65 ± 0.02, m_{Se} = 6.6 × 10^{-3} mol kg^{-1}, m_{Na+} = 0.96 mol kg^{-1}, 25.3 °C).

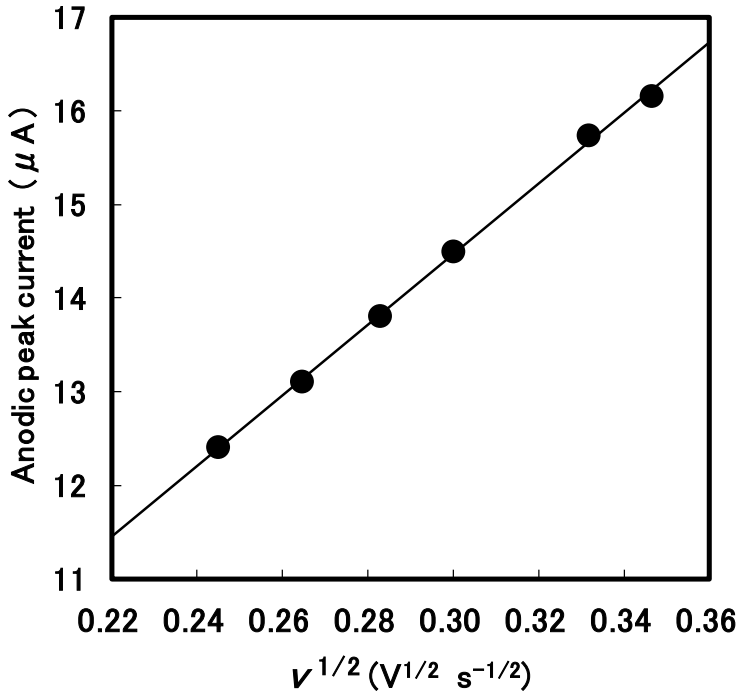

Figure 3. 8. Dependence of the anodic peak current on $v^{1/2}$. The six filled circles corresponding to each scan rate in the figure are obtained from the 40th cyclic voltammogram after repetitive potential cycling measured in a solution containing SeO_3^{2-}. The solid line is the linear least-squares fit of data. The linear dependence of the anodic peak current on $v^{1/2}$ is indicative of the diffusion-controlled process.

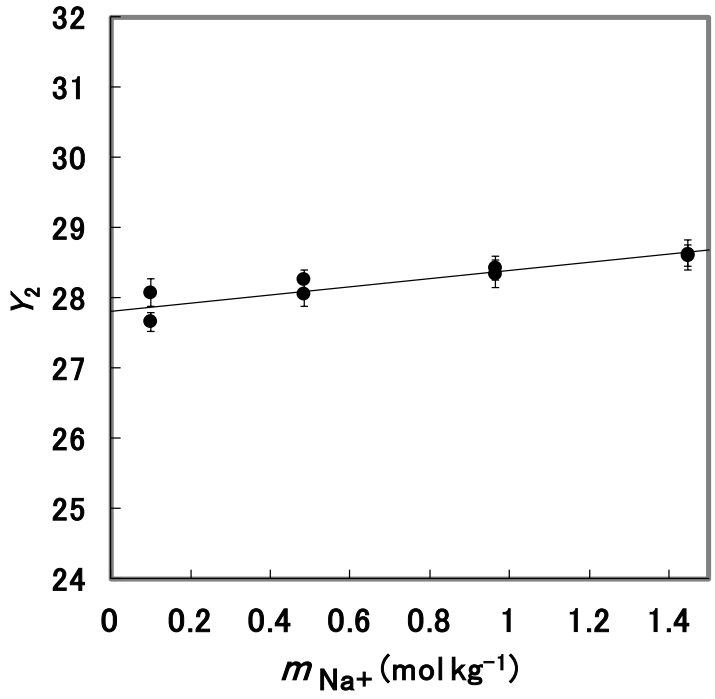

Figure 3. 9. Determination of the standard redox potential for the SeO_4^{2-}/SeO_3^{2-} couple using the specific ion interaction theory. Experimental data as a function of m_{Na+} is shown as the filled circle. The solid line is the weighted linear regression fit [21] of data. The slope and intercept of this line correspond to $\Delta\varepsilon_2$ and $E_{SeO4\ 2-/SeO3\ 2-}(T_0, 0)/J$, respectively. $Y_2 = \{E_{1/2}(T_0, I_m) + E_{Ref}(T_0, I_{Ref})\}/J - 2\log a_{H+} + \log a_{H2O}$, where $J = RT/2F \log e$.

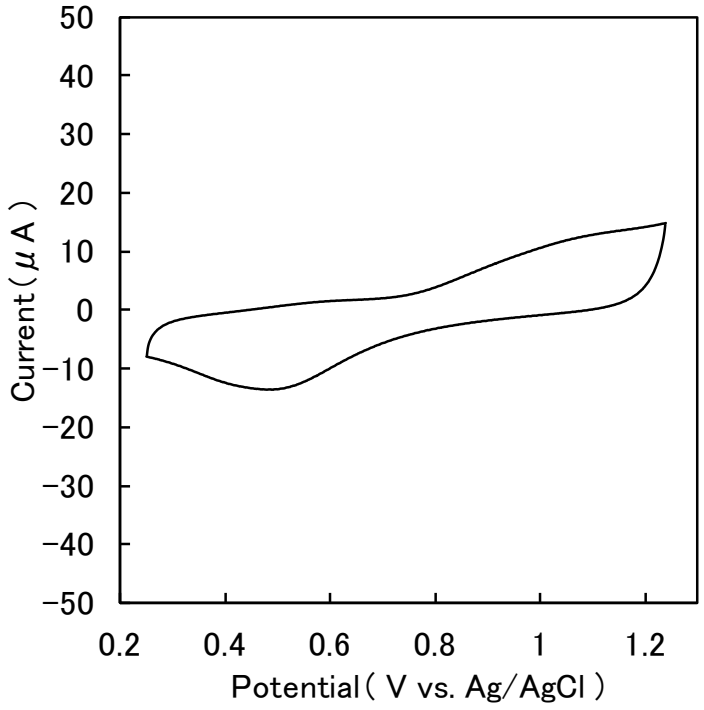

Figure 3. 10. Cyclic voltammogram of the blank solution ($-\log a_{H+}$ = 1.11, m_{Na+} = 2.00 mol kg^{-1}, 25.5 °C).

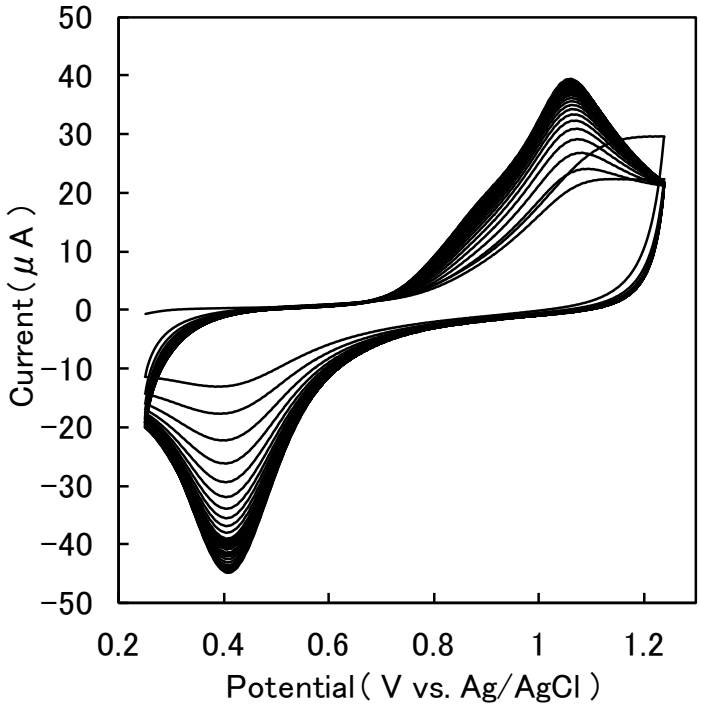

Figure 3. 11. Cyclic voltammogram of a solution containing H_2SeO_3 after repetitive potential cycling ($-\log a_{H^+}$ = 1.11, m_{Se} = 9.3 × 10^{-4} mol kg^{-1}, m_{Na^+} = 2.00 mol kg^{-1}, 15.5 °C).

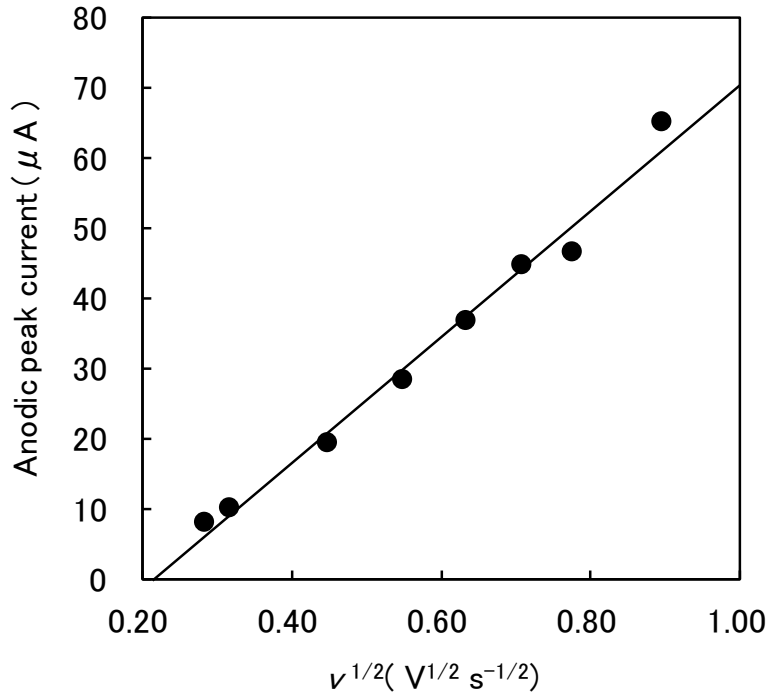

Figure 3. 12. Dependence of the anodic peak current on $v^{1/2}$. The eight filled circles corresponding to each scan rate in the figure are obtained from the 40th cyclic voltammogram after repetitive potential cycling measured in a solution containing H_2SeO_3 ($-\log a_{H^+}$ = 1.15, m_{Na^+} = 1.00 mol kg^{-1}, 24.5 °C). The solid line is the linear least-squares fit of data. The linear dependence of the anodic peak current on $v^{1/2}$ is indicative of the diffusion-controlled process.

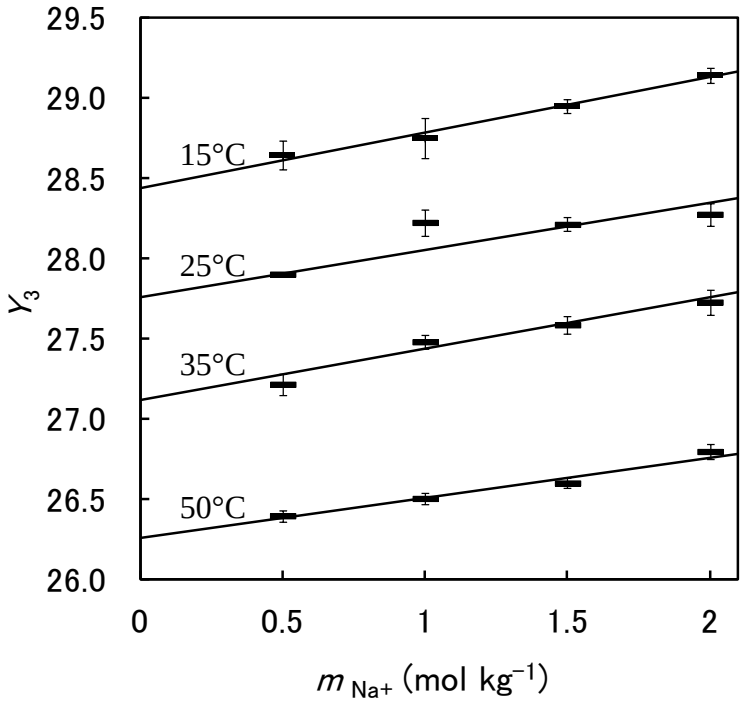

Figure 3. 13. Determination of the standard redox potential of the $HSeO_4^-/H_2SeO_3$ couple using the specific ion interaction theory. Experimental data as a function of m_{Na+} is shown as the solid bars with a vertical bar showing the standard deviation in each data point. The solid line is a weighted linear regression [21] of data. The slope and intercept of each line correspond to $\varepsilon_T(HSeO_4^-, Na^+)$ and $Y_{intercept}$, respectively, at each temperature. $Y = E_{1/2}^{ave}(T, I_m)/J + D(T, I_m) - 3\log a_{H+} + \log a_{H2O}$, where $J = RT/2F \log e$.

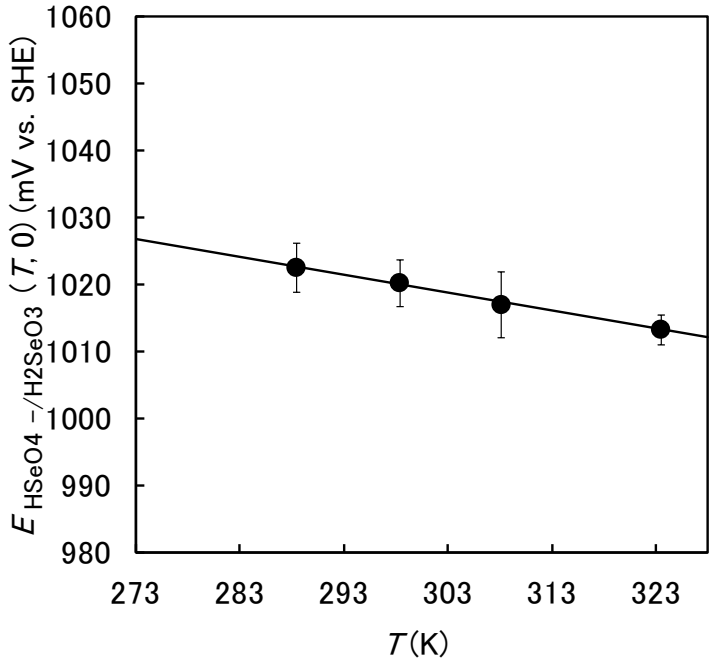

Figure 3. 14. Determination of the molar entropy of the $HSeO_4^-/H_2SeO_3$ couple. The $HSeO_4^-/H_2SeO_3$ standard redox potential as a function of temperature is shown as the filled circle with vertical bar showing the standard deviation in each data point. The solid line is a weighted linear regression [21] of data. The slope of this line corresponds to $\Delta_r S^0_m /2F = -0.3 \pm 0.1$ mV °C^{-1}.

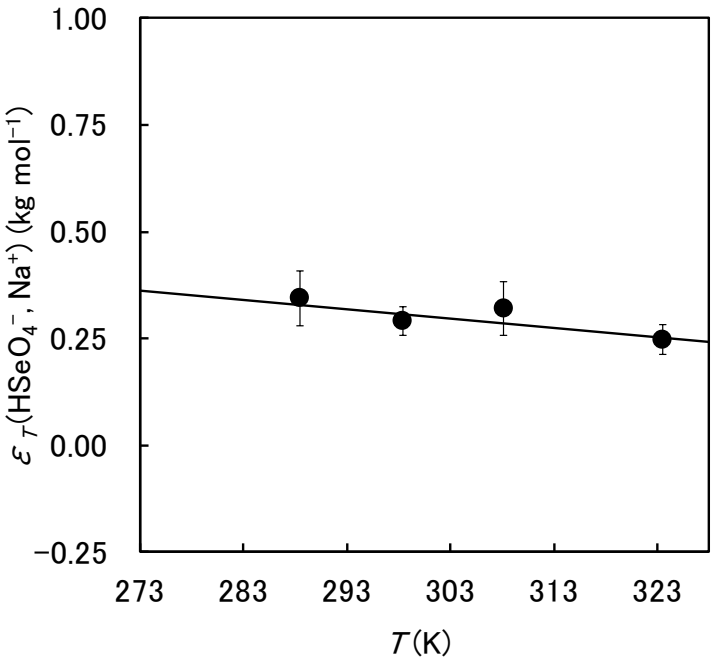

Figure 3. 15. Dependence of the ion interaction coefficient $\varepsilon_T(HSeO_4^-, Na^+)$ on temperature. The ion interaction coefficient $\varepsilon_T(HSeO_4^-, Na^+)$ as a function of temperature is shown as the filled circle with vertical bar showing the standard deviation in each data point. The solid line is a weighted linear regression [21] of data. The slope of this line corresponds to $\partial\varepsilon/\partial T = -0.002 \pm 0.002$ kg mol^{-1} °C^{-1}.

Chapter 4. General conclusions

The accurate prediction of the solubility and speciation of Se in groundwater is required for the safety assessment of the geological disposal system. The investigations of Se species have been carried out for the purpose of obtaining the information on the solubility-limiting solid phase of Se and the standard thermodynamic data for Se, because they are crucial for the calculation of the solubility and speciation of Se using thermodynamic models. Because the migration behavior of Se significantly depends on the redox potential, it is necessary to estimate the solubility and speciation of Se in oxidized groundwater as well as in reducing groundwater. The information on the solubility-limiting solid phase of Se, which is essential for the calculation of the Se solubility in reducing groundwater, was obtained in Chapter 2. The standard thermodynamic data of the Se(VI)/(VI) couple, which determine the Se speciation in oxidized groundwater, were obtained in Chapter 3. The obtained results are summarized as follows:

In Chapter 2, two Se solubility experiments were performed in the presence of Fe under reducing conditions. The first used the bentonite equilibrated water and the second the water without bentonite. In bentonite equilibrated waters, the experimental conditions fell into the stability field of $FeSe_2$(cr) when plotted on a potential-pH diagram, although no Se solid phases were identified. Using the pure water experiment, the experimental conditions constantly fell into the stability field of $FeSe_2$(cr) when plotted on a potential-pH diagram. After 1 month the experimental system was under a transitional condition, moving toward true equilibrium from over-saturation, and the solid phase which decreased the Se concentrations was likely to be $FeSe_2$(cr). Se(cr) did not control the Se concentrations because the Se concentrations was lower than its solubility, even though the XRD patterns indicated that Se(cr) was the dominant solid phase. After 2 months and 3.5 months, Se(cr)

transformed to Fe-Se solid phase ($FeSe_2$(cr) and FeSe(cr)). The transformation from Se(cr) to Fe-Se solid phase ($FeSe_2$(cr) and FeSe(cr)) with the increase in aging period was observed by the XRD. The formation of $FeSe_2$(cr) is likely to be caused in the long term by the presence of Fe, resulting from carbon steel overpack corrosion in the engineered barrier systems under reducing conditions.

In Chapter 3, electrochemical investigations, using cyclic voltammetry, has been carried out to determine the standard redox potentials of the following redox reactions:

$$SeO_4^{2-} + 3H^+ + 2e^- \rightleftharpoons HSeO_3^- + H_2O, \quad (4\text{-}1)$$

$$SeO_4^{2-} + 2H^+ + 2e^- \rightleftharpoons SeO_3^{2-} + H_2O. \quad (4\text{-}2)$$

The Se(VI)/(IV) half-wave potentials were measured as a fuction of m_{Na+}. Extrapolation of the experimental data to $m_{Na+} = 0$ using SIT yields the following standard redox potentials:

$E_{SeO4\ 2-/HSeO3\ -}(T_0, 0) = 1.074 \pm 0.011$ V vs. SHE,

$E_{SeO4\ 2-/SeO3\ 2-}(T_0, 0) = 0.8227 \pm 0.0032$ V vs. SHE.

Excellent agreement among $E_{SeO4\ 2-/HSeO3\ -}(T_0, 0)$, $E_{SeO4\ 2-/SeO3\ 2-}(T_0, 0)$ and the corrected value of the equilibrium constant of the following reaction

$$Br_2 + H_2SeO_3 + H_2O \rightleftharpoons 3H^+ + HSeO_4^- + 2Br^-, \quad (4\text{-}3)$$

was found. In addition, another electrochemical investigation has been carried out to determine the molar entropy of the Se(VI)/(IV) couple, which provides the accurate prediction of the Se speciation at a temperature over 25 °C. To obtain the value for $\varepsilon_T(HSeO_4^-, Na^+)$, the following reaction involving $HSeO_4^-$ as the oxidant and the H_2SeO_3 uncharged species as the reductant was used:

$$HSeO_4^- + 3H^+ + 2e^- \rightleftharpoons H_2SeO_3 + H_2O\ . \quad (4\text{-}4)$$

The Se(VI)/(IV) half-wave potentials were measured as functions of m_{Na+} and temperature ranging from 15 to 50 °C. The following molar entropy was derived from the temperature

dependence of $E_{\mathrm{HSeO4\ -/H2SeO3}}(T_0, 0)$:

$\Delta_r S^0{}_m / 2F = -0.3 \pm 0.1$ mV °C $^{-1}$.

The obtained values of $\Delta_r S^0{}_m$ and $\Delta_r G^0{}_m$ of Equation (4-4) were consistent with the $\Delta_r H^0{}_m$ value calculated from the OECD/NEA-selected values. The value of $\varepsilon_T(HSeO_4^-, Na^+)$ at 25 °C was determined to be 0.29 ± 0.03 kg mol^{-1}. The following $\partial\varepsilon/\partial T$ was derived from the temperature dependence of $\varepsilon_T(HSeO_4^-, Na^+)$:

$\partial\varepsilon/\partial T = -0.002 \pm 0.002$ kg mol^{-1} °C $^{-1}$,

consistent with the previous studies of $\partial\varepsilon/\partial T$.

The accurate prediction of the solubility and speciation of Se in groundwater supports the safety assessment of the geological disposal system. Owing to the important and useful information obtained by Se solubility experiments in Chapter 2, $FeSe_2$(cr) can be chosen as the solubility-limiting solid phase of Se for the calculation of the Se solubility in reducing groundwater. Using a thermodynamic database including the standard redox potential and the molar entropy of the Se(VI)/(IV) couple obtained in Chapter 3, the Se(VI)-to-Se(IV) ratios at a temperature over 25 °C in oxidized groundwater can be accurately calculated. This thesis has provided the important information on the solubility-limiting solid phase of Se and the standard thermodynamic data for Se.

Acknowledgement

I would like to express my deep gratitude to my supervisor Professor Gento Kamei (Division of Material Sciences, Graduate School of Natural Science and Technology, Kanazawa University) and Professor Akihiko Yokoyama (Division of Material Sciences, Graduate School of Natural Science and Technology, Kanazawa University) for many discussions, suggestions, continuous encouragement and support throughout this study.

I am greatly indebted to Professor Jyun'ichi Sakai (Waseda University), Dr Yoshikawa (Japan Atomic Energy Agency), Dr Ishidera (Japan Atomic Energy Agency), Dr Fujiwara (Japan Atomic Energy Agency) and Dr Yoshida (NESI) for the advice on receiving a doctoral degree.

Finally, I would like to thank my wife, daughter and parents for their warm encouragement and supports.

List of publications

Chapter 2

Doi R, Tachikawa H, Yui M. [Transformation of selenium solid phase in the presence of iron under reducing conditions]. J. Nucl. Sci. Technol. 2010; 47 No.3:278-285.

Chapter 3

Doi R, Yui M. [Experimental study by cyclic voltammetry of standard potential of Se(IV)/Se(VI) redox system]. Journal of Nuclear Fuel Cycle and Environment. 2009; 16 No. 1:35-42 [in Japanese].

Doi R. [Errata to "Experimental study by cyclic voltammetry of standard potential of Se(IV)/Se(VI) redox system"]. Journal of Nuclear Fuel Cycle and Environment. 2012; 19 No. 2:65-66 [in Japanese].

Doi R. [Determination of the selenium (VI)/(IV) standard redox potential by cyclic voltammetry]. J. Nucl. Sci. Technol. 2014; 51 No.1:56-63. (published online: 21 Oct 2013)

Doi R. [Molar entropy of the selenium (VI)/(IV) couple obtained by cyclic voltammetry]. J. Nucl. Sci. Technol. (published online: 9 January 2014)